ISSN/2499-5347

F. ADDESA
Princeton University

M. CAMPANA, D. DEL RE, B. D'ORSI, R. PARAMATTI, F. SANTANASTASIO, R. TRAMONTANO
INFN Rome
Sapienza University, Roma

I. DAFINEI, E. DI MARCO, P. MERIDIANI, C. ROVELLI, L. SOFFI
INFN, Rome

A. CEMMI, I. DI SARCINA, G. FERRARA
Fusion and Technology for Nuclear Safety and Security Department
Innovative Nuclear Systems Laboratory
Casaccia Research Centre, Rome - Italy

OPTICAL SPECTROSCOPIC CHARACTERIZATION OF LYSO CRYSTALS AT THE CALLIOPE FACILITY (ENEA CASACCIA R.C.)

RT/2020/15/ENEA

ITALIAN NATIONAL AGENCY FOR NEW TECHNOLOGIES,
ENERGY AND SUSTAINABLE ECONOMIC DEVELOPMENT

F. ADDESA
Princeton University

M. CAMPANA, D. DEL RE, B. D'ORSI,
R. PARAMATTI, F. SANTANASTASIO,
R. TRAMONTANO
INFN Rome
Sapienza University, Roma

I. DAFINEI, E. DI MARCO, P. MERIDIANI,
C. ROVELLI, L. SOFFI
INFN, Rome

A. CEMMI, I. DI SARCINA, G. FERRARA
Fusion and Technology for Nuclear Safety
and Security Department
Innovative Nuclear Systems Laboratory
Casaccia Research Centre, Rome - Italy

OPTICAL SPECTROSCOPIC CHARACTERIZATION OF LYSO CRYSTALS AT THE CALLIOPE FACILITY (ENEA CASACCIA R.C.)

RT/2020/15/ENEA

ITALIAN NATIONAL AGENCY FOR NEW TECHNOLOGIES,
ENERGY AND SUSTAINABLE ECONOMIC DEVELOPMENT

OPTICAL SPECTROSCOPIC CHARACTERIZATION OF LYSO CRYSTALS AT THE CALLIOPE FACILITY (ENEA CASACCIA R.C.)

F. Addesa, M. Campana, A. Cemmi, I. Dafinei, D. del Re, E. di Marco, I. Di Sarcina, B. D'Orsi, G. Ferrara, P. Meridiani, R. Paramatti, C. Rovelli, F. Santanastasio, L. Soffi, R. Tramontano

Riassunto

I cristalli scintillanti di LYSO sono ampiamente utilizzati in esperimenti di fisica. Il presente Rapporto Tecnico riguarda la caratterizzazione ottica e spettroscopica di cristalli di LYSO di dodici diversi ri-venditori. A questo scopo sono state effettuate misure di fotoluminescenza e trasmittanza nel range UV-VIS, prima e dopo irraggiamento a 50 kGy, per verificare la resistenza alla radiazione dei cristalli.

Parole chiave: irraggiamento gamma, cristalli di LYSO, rivelatori a scintillazione, resistenza a radiazione.

Abstract

LYSO scintillating crystals are widely used in physics experiment. The present Technical Report regards optical and spectroscopic characterization of LYSO crystals of twelve different producers. Photoluminescence and UV-VIS transmittance were studied, before and after irradiation up to 50 kGy absorbed dose, to investigate the radiation resistance of the crystals.

Keywords: *gamma irradiation, LYSO crystal, scintillating detector, radiation hardness.*

INDEX

Introduction

The present Technical Report regards the characterization of LYSO scintillating crystals doped with Cerium (LYSO:Ce) through optical and spectroscopic techniques. LYSO:Ce is an inorganic compound used as scintillator, widely employed in radiation detection. LYSO:Ce crystals are characterized by small rise time and decay time, high light yield, good radiation resistance and high density, i.e. short radiation length and availability on the market. The analysed crystals have dimensions ~3x4x57 mm. LYSO:Ce high radiation tolerance is a fundamental feature when it is used as scintillator, coupled to a light detector, in high energy physics experiments.

Given the large number of LYSO:Ce producers and the variety of material offered, a screening of LYSO:Ce crystals from different producers is presented in this report.

This work is focused on the optical spectroscopic characterization of LYSO:Ce crystals from twelve different vendors, before and after irradiation up to 50 kGy absorbed dose, to test their radiation resistance. Annealing treatments after irradiation were also performed in order to study the crystals transmittance recovery.

In the first chapter, the fundamental features of LYSO:Ce crystal and the scintillation mechanism are presented together with the experimental setup.

In the second chapter, the obtained photoluminescence and UV-VIS transmittance spectra are shown, before and after irradiation up to 50 kGy absorbed dose. The results obtained after annealing treatments are also reported.

1 Materials and methods

The analysed LYSO:Ce producers, in alphabetic order, are:

- Crystal Photonics, USA
- EPIC Crystal, China
- Hamamatsu Photonics, Japan
- Hypercrystal, Taiwan
- JT Crystal Technology, China
- Saint-Gobain, France
- Shangai EBO Optoelectronics, China
- Shangai Institute of Ceramics, China
- Simcrystals Technology, China
- SIPAT, China
- Tianle Photonics, China
- Zecotek Imaging System, Singapore

Experimental measurements discussed here were carried out at the Calliope gamma irradiation facility at ENEA Casaccia research centre. LYSO:Ce crystals were characterized by optical-spectroscopic techniques (UV-Vis transmission, emission and excitation spectra) before and after irradiation steps at different absorbed doses.

1.1 LYSO:Ce crystal

Lutetium-yttrium oxyorthosilicate crystal doped with Cerium ($(Lu_{1-x}\,Y_x)_2\,SiO_5 : Ce$), abbreviated as LYSO:Ce, is an inorganic compound used as scintillator. LYSO:Ce crystals have attracted a broad interest in the high energy physics community because of their properties. They are suitable for precision timing measurement because they are characterized by a high light yield (~40000 photons/MeV), a fast scintillation rise time (<100 ps), and relatively short decay time (~40 ns) as measured in [1].

The LYSO:Ce compound has high density and a radiation length $X_0 = 1.14\ cm$ thus minimizing the required thickness when used as scintillator.
A key feature of LYSO:Ce is its radiation tolerance, which is required in order to operate without significant loss of transparency, and consequent decrease of the light yield, also in the high radiation environment.

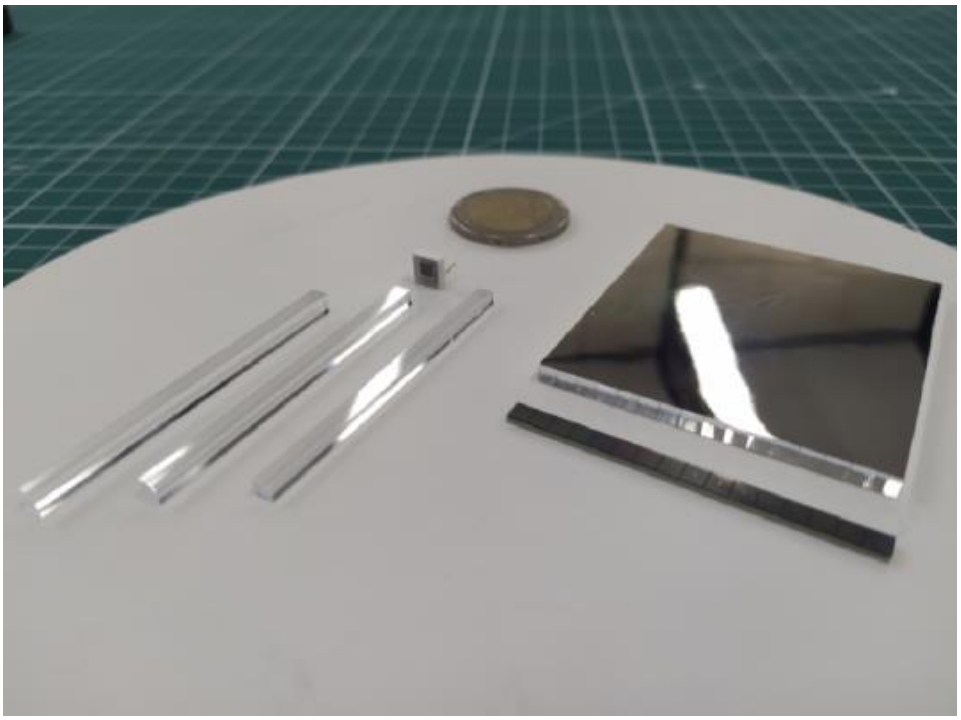

Figure 1 - LYSO:Ce bars of different size and an array of 16 bars.

1.1.1 The scintillation mechanism

An ideal scintillating material has to satisfy different criteria i.e. it should have a high scintillation efficiency, it must provide a signal proportional to the deposited energy, it should be transparent to the emitted light and it must have a short decay time thus fast light pulses can be generated.
Scintillator working principle is based on the emission of light from the scintillating material after its excitation due to radiation exposure. If the emission occurs immediately after the absorption (within $\sim 10^{-8}\, s$), the process is usually called fluorescence. However also processes such as phosphorescence, characterized by a much longer emission time, could happen.

Inorganic scintillators are generally made of a crystal or glass matrix, in which luminescence comes from emission centres already present in the structure, or from activator agents introduced in the crystal lattice in controlled way. A scheme of a typical electronic band structure is shown in Fig. 2 [2].

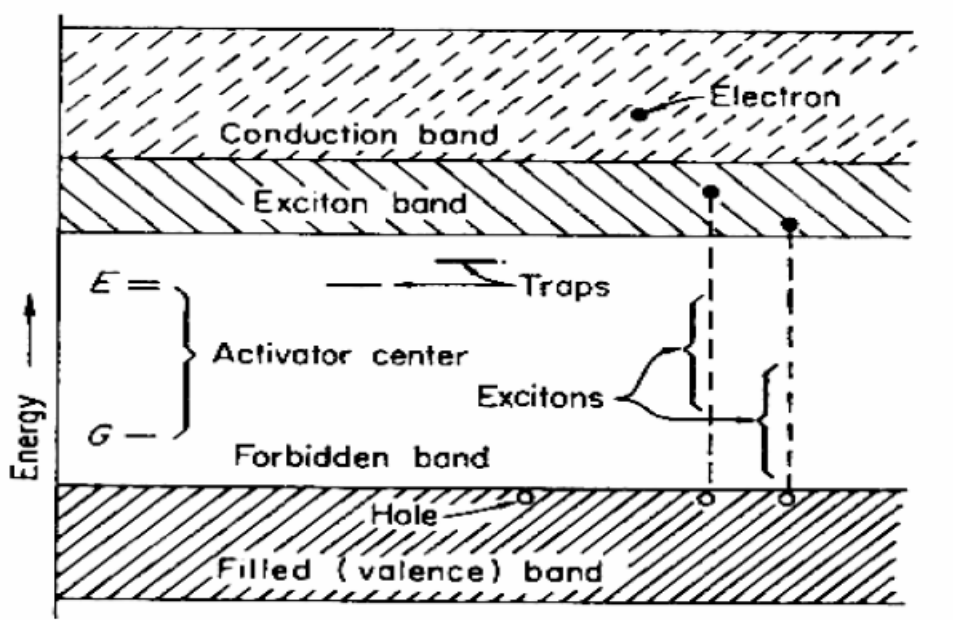

Figure 2 - Energy band model of a scintillator.

From the point of view of their possible involvement in a luminescence process, the defect centres can be divided in:

- Luminescent centres: the transition to the ground state is accompanied by the emission of a photon;
- Quenching centres: the energy is dissipated through radiationless processes;
- Traps: metastable levels from which the electrons can reach the conduction band, by acquiring thermal energy from the lattice vibrations, or fall into the valence band by a radiationless transition.

The luminescence and quenching centres arise from impurities, interstitial ions and defects, and they introduce local discrete energy levels corresponding to the ground and excited states of the centre.
Small amount of doping agent can be added to inorganic scintillators in order to enlarge the probability of having a photon emission when the transition to the ground state occurs (Fig. 3). In this way, the nominal band structure is modified and as a result, there will be energy states created within the forbidden gap through which the luminescence centre can de-excite.

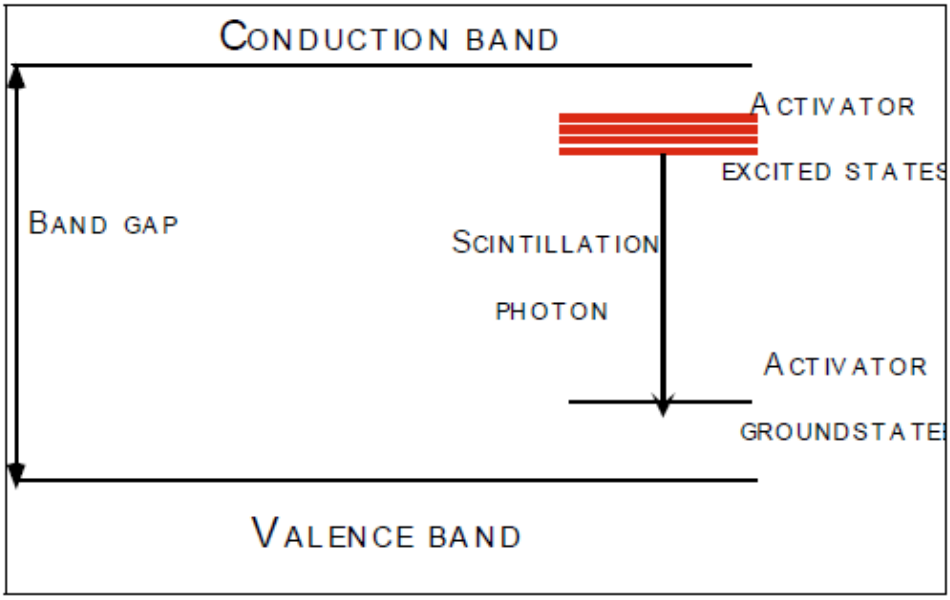

Figure 3 - Energy band structure of an impurity-activated scintillating crystal.

When a charged particle passes through matter, it loses its energy via excitation and ionization, i.e. can release enough energy to an electron allowing it to move to the conduction band. This mechanism gives rise to the creation of an electron-hole pair. If the electron passes near one of the activator centres, can drop into it, creating a neutral impurity configuration which can have its own set of excited energy states. If the activator state thus formed, is an excited configuration with an allowed transition to the ground state, its de-excitation will happen with a high probability through the emission of a photon. If the activator is properly chosen, this transition can be in the visible energy range.

The luminescent centres in LYSO:Ce crystal are due to Ce^{3+} and Ce^{4+} ions. The light yield (LY) of the crystal increases as the cerium concentration increases until it reaches its maximum value and then, because of self-absorption effect, the LY is quenched. In Ce-doped crystal, the scintillation mechanism consists in the trapping of a hole by Ce^{3+} forming temporary Ce^{4+}, followed by the capture of a free electron resulting in Ce^{3+} in an excited state. The latter de-excites radiatively giving a blue photon characteristic of the $5d \rightarrow 4f$ transition [3] (Fig. 4).

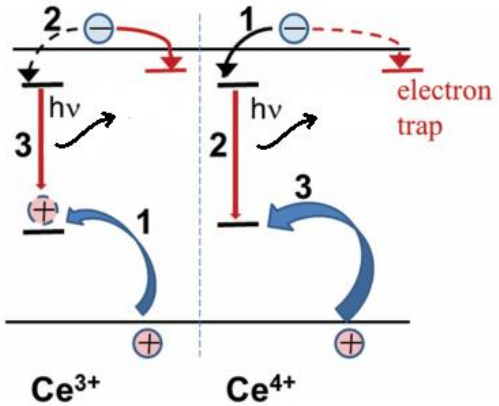

Figure 4 - Scheme of the scintillation mechanism at the stable *Ce*3+ and *Ce*4+ luminescence centres [4].

Scintillation mechanism can be summarized in three steps: absorption of the incident radiation, conversion of energy in electron-hole pairs, which in turn transfer their energy to the luminescent centres, and emission. The first stage of scintillation depends on the way a charged particle, or a high energy radiation, interacts with matter and it is described, together with the other scintillation steps, in the next sections.

Absorption

The intensity of a monoenergetic beam of -rays entering a detector of thickness *d* is reduced according to:

$$I = I_0 e^{-\mu_l d} \tag{1}$$

where μ_l is the linear absorption coefficient of the material and it depends on electron density and absorption cross section σ_e. The main processes by which photons interact with matter are: photoelectric effect, Compton effect and pair production.

The total cross section can be expressed as follows:

$$\sigma_e = \sigma_{ph} + \sigma_C + \sigma_{pp} \tag{2}$$

where σ_{ph}, σ_C and $\sigma_{pp}$are the cross section respectively of photoelectric effect, Compton effect and pair production [5]. The energy range at which each process dominates is shown in Fig. 5 as a function of the atomic number Z of the absorber.

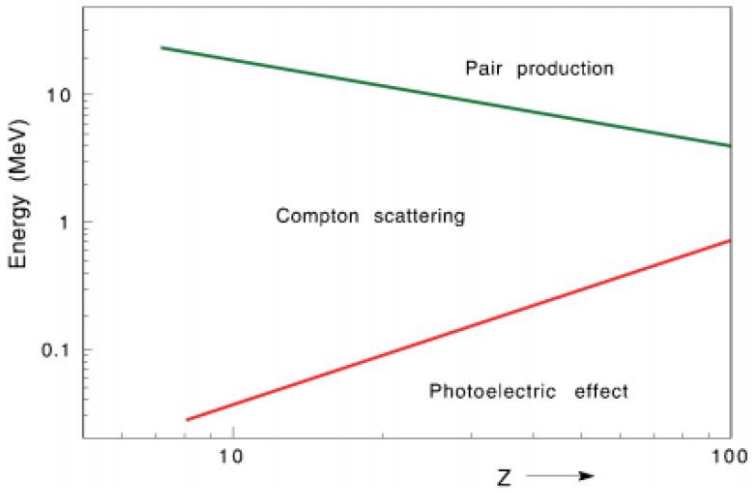

Figure 5 - Possible processes happening when photons cross a material.

In the photoelectric effect the photon is absorbed by an atom which in turn emits an atomic electron, called photoelectron. The photoelectron kinetic energy E_{pe} is equal to the difference between the energy of the impinging photon $E_\gamma = h\nu$ and the electron binding energy E_b:

$$E_{pe} = E_\gamma - E_{pe} \tag{3}$$

A part of the photon momentum has to be passed to the atom, in order to have photoelectric effect.

The Compton effect is the scattering of a photon by a bound electron that acts as a free electron. In the final state there are a photon, whose direction is different with respect to the incident one, and an electron with a kinetic energy determined by the energy and momentum conservation laws.

At high energy, starting from the energy threshold value $E_\gamma > 2m_e c^2$, the most probable process is the pair production in which a photon is converted into an electron-positron pair.

A charged particle loses its energy in a material according to the Bethe-Bloch formula:

$$-\frac{1}{\rho}\frac{dE}{dx} = \frac{4\pi N_A r_e^2 mc^2 z^2}{\beta^2}\frac{Z}{A}\left[\ln\left(\frac{2mc^2\beta^2\gamma^2}{I}\right) - \beta^2\right] \quad (4)$$

where m, z and β are respectively the mass, charge and velocity of the particle, r_e is the classical electron radius, N_A is the Avogadro number, I is the mean ionization potential of the traversed medium and Z its atomic number. In Fig. 6, the energy loss is reported as a function of impinging particle $\beta\gamma$.
The particles for which the energy loss is close to the minimum are called minimum ionizing particle (MIP).

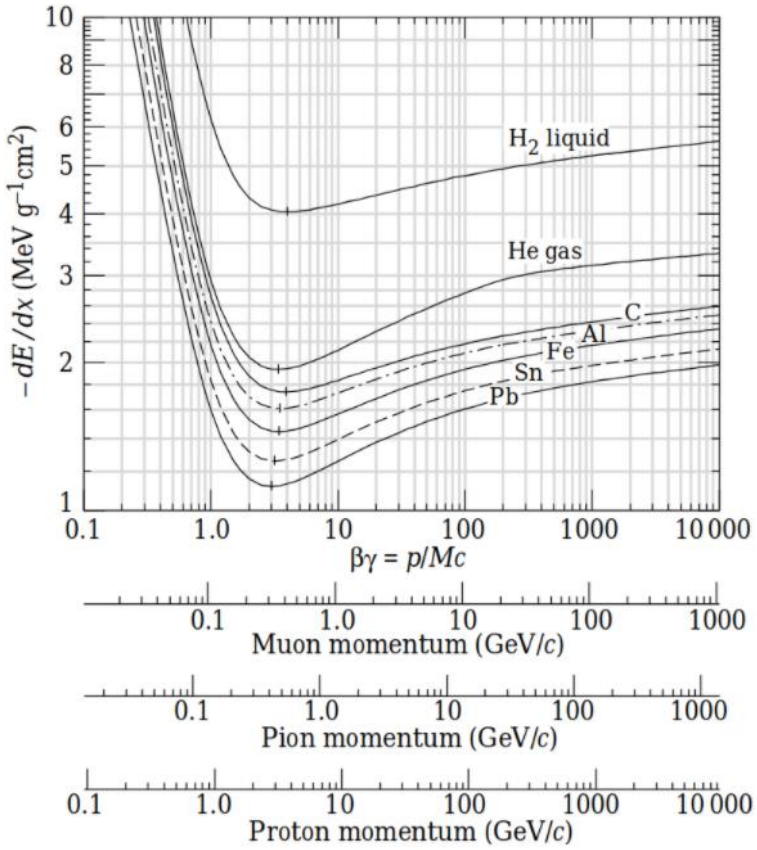

Figure 6 - Energy loss by charged particles due to ionization.

Positrons and electrons lose their energy in matter by ionization and *bremsstrahlung* (radiation). The former process dominates at low energy while the latter at high energy.

Conversion

When the incident high radiation is absorbed, it creates electron-hole pairs which may transfer their energy to the luminescent centre. An important feature of the scintillators for this stage, is the scintillation effectiveness ϵ_s defined as the number of emitted photons for 1 MeV of deposited energy.

For a crystal with a band gap E_g, it is possible to define the energy needed in order to create an electron-hole pair E_{eh} as:

$$E_{eh} = \beta E_g \tag{5}$$

where $\beta > 1$. Thus, the number of electron-hole pair N_{eh} can be obtained if the photon energy is known, in fact:

$$N_{eh} = \frac{E_\gamma}{E_{eh}} \tag{6}$$

where E_γ is the absorbed energy. By considering the number of emitted photons N_{ph} which is proportional to N_{eh}, to the efficiency of the transfer from electron-hole pair to the luminescent centre S and to the luminescence efficiency of the centre q, the scintillation effectiveness can be written as:

$$\epsilon_s = \frac{N_{ph}}{E_\gamma} = \frac{Sq}{\beta E_g} \tag{7}$$

Therefore, in order to have a good scintillator, q and S must be close to 1 while the product βE_g must be as little as possible.

Emission

After the conversion process, the luminescent centre is in an excited state. The scintillation process occurs if the centre goes back to its ground state emitting a visible photon. The emission spectrum shape varies depending on the atomic configuration of the crystal. For example, the $5d \rightarrow 4f$ transition of Ce^{3+} causes a band emission spectrum.

1.1.2 Radiation effects in solids

The interaction of ionizing radiation with a scintillating crystal, causes radiation damage. Optical properties of a scintillator can change after irradiation. For example, during irradiation some electrons can move away from crystal ion, creating

an electron-hole pair. If an electron passes near a positive charged defect before the recombination, it can remain bound to the defect because of its Coulomb field. In the same way, a hole can be entrapped from negative charged defects. The resulting entity is called "colour centre", since it can absorb visible light, and it causes the optical transmission to decrease.

It has been demonstrated that UV-Vis absorption can be decreased by the presence of cerium in crystal and glass matrix [6] of different composition. Indeed, cerium ions, which have absorption bands in the deep UV, act as traps for the ionizing radiation-induced holes and electrons [7]. However, the degrading effects in the visible range cannot be completely removed [8] [9].

Cerium ions in glass are normally found both in the Ce^{3+} and Ce^{4+} states. The positions of the absorption bands of these states in the UV range, depend on the crystal matrix composition.

The reactions that take place in the cerium-doped crystal matrix, after irradiation, are:

$$Ce^{3+} + h \rightarrow \ Ce^{3++} \tag{8}$$

$$Ce^{4+} + e \rightarrow \ Ce^{3+} \tag{9}$$

Ce^{3++} is essentially a Ce^{4+} and it shows an absorption band close to 250 nm [8] [10].
In most crystals, an observed loss in light yield after irradiation, can be explained by a decrease in transmission rather than in luminescence, as shown in a lot of research [5]. Therefore, the radiation tolerance studies in this work, are focused on measuring the optical transmission of LYSO:Ce crystals after irradiation.

The Light Yield (LY) is one of the most important features characterizing a scintillator. The photons created in the scintillator are affected by many processes that reduce their number before reaching the entrance of the photo-device. Therefore, the size of the scintillator crystal and its self-absorption, the transmittance of the crystal, the quality of the reflector material, have to be considered [11], in the LY evaluation. It corresponds to the number of photons emitted by the scintillator that arrive on the photocathode of the PMT for 1 MeV of deposited energy. Its value is expressed in photons per MeV (ph/MeV). The numbers of photons can be converted into numbers of photoelectrons using the quantum efficiency of the photomultiplier.
The time interval between the absorption of ionizing radiation and emission of scintillation light (photons), depends on the material. It can vary in a wide range from picoseconds, in fast scintillators, to seconds and more, in the case of phosphors.
The number of emitted photons can be described by the sum of two exponentials corresponding to the rise time and decay time:

$$N(t) = \frac{N_{ph}}{DT-RT}\ (e^{-\frac{t}{DT}} - \ e^{-\frac{t}{RT}}) \tag{10}$$

where N_{ph} is the total number of emitted photons and DT and RT are the decay and rise time, respectively. However, the promotion of excited electrons to upper energy levels, which includes both absorption and conversion process, is considered to be faster than the final emission of scintillation light. Therefore, in order to describe the time evolution of the re-emission process, the RT can be usually neglected in most materials with respect to the DT. In this approximation, the number of emitted photons shows a single exponential dependence on time:

$$N(t) = \frac{N_{ph}}{DT}\ e^{-\frac{t}{DT}} \tag{11}$$

The DT is defined as the time after which the number of emitted photons from a scintillating material, is decreased of a factor 1e with respect to the total number N_{ph}.
Another important feature for a scintillating material is the transparency to its fluorescent radiation which will be discussed in Chapter 3.

1.2 Calliope gamma irradiation facility

The Calliope gamma irradiation facility is a pool-type facility equipped with a ^{60}Co radio-isotopic source array in a large volume (7.0x6.0x3.9 m) shielded cell [12]. The source rack is composed of 25 ^{60}Co source rods (with an active area of 41x90 cm) placed in a planar geometry (Fig. 7).

Figure 7 - a) Calliope source rack in the pool and b) source rack within the irradiation cell (picture acquired by remote camera).

In a simplified decay scheme of ^{60}Co, two photons of 1.17 MeV and 1.33 MeV are emitted in coincidence, (Fig. 8).

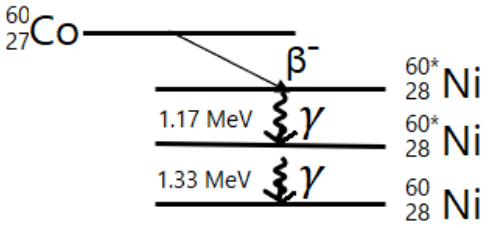

Figure 8 - Simplified ^{60}Co decay scheme.

The physical quantity which gives a quantitative correlation between radiation and its effects, is the absorbed dose. It is defined as the ratio between the energy released from radiation in a certain volume of the matter and the mass contained in that volume. In the International System of Units (SI), the absorbed dose is measured in Gray (Gy):

$$1Gy = 1\,\frac{J}{kg} \tag{12}$$

The absorbed dose per time unit represents the dose rate. The present activity for the Calliope plant is $1.97 \cdot 10^{15}$ Bq and, positioning a sample at different distances with respect to the source rack, within the irradiation cell, it is possible to irradiate it at different dose rate values; in particular the maximum available dose rate is 7.87 kGy/h. The steel platform, shown in Fig. 7.b, is installed to perform irradiation at high dose

rate values. The storage pool dimensions are 2.0x4.5x8.0 m with two separate emergency-storage wells at the bottom.

1.3 Transmittance measurements

Transmittance (T,%) and fluorescence measurements are useful to investigate the LYSO:Ce crystal behaviour. Transmittance is the ratio between the intensity of the beam that passes through the crystal, which is decreased of a factor $(1-R)^2 e^{-\alpha d}$, and the intensity of the incidence beam (I_0):

$$T = \frac{I_0(1-R)^2 e^{-\alpha d}}{I_0} \tag{13}$$

where R and α are the reflection and the absorption coefficients and d is the crystal optical path. This formula takes into account the effect of the multiple reflections on both faces of the sample.

Transmittance spectra were measured by a Perkin Elmer UV/Vis/NIR Lambda 900 spectrophotometer equipped with a double beam (Fig. 9) and a general purpose optical bench.

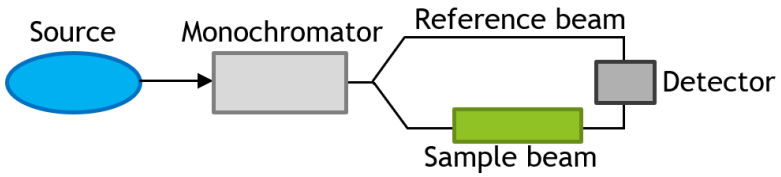

Figure 9 - Double beam spectrophotometer scheme.

The optical transmission in a double beam spectrophotomer is defined as:

$$T = \frac{\frac{S-D}{Ref-D}}{\frac{S_0-D_0}{Ref_0-D_0}} \tag{14}$$

where S, Ref and D are respectively the measured, reference and dark signal values and the index 0 is referred to the baseline acquired at the beginning of a set of measurements with the sample holder positioned inside the sample compartment of the instrument, without the crystal sample. Longitudinal and transversal transmittance measurements were performed with the crystal placed on a dedicated sample holder in two different position with respect to the incident beam, as shown in (Fig. 10).

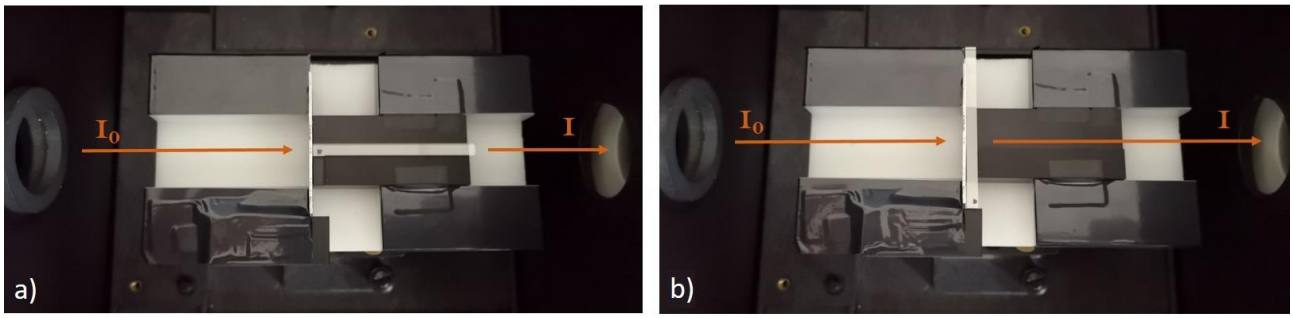

Figure 10 - LYSO:Ce crystal positioned in the customized sample holder for a) longitudinal measurements and b) transversal measurements. The crystal dimensions are: 3.12x57x3.75 mm. The orange lines show the incident and the outgoing beam.

Thermal annealing treatments were performed using a Thermo Scientific KÖNN LAB-01/400 Furnace. The crystals were treated at 300 °C in air for 16 hours, with heating and cooling rate of 4.6 °C/min (Fig. 11).

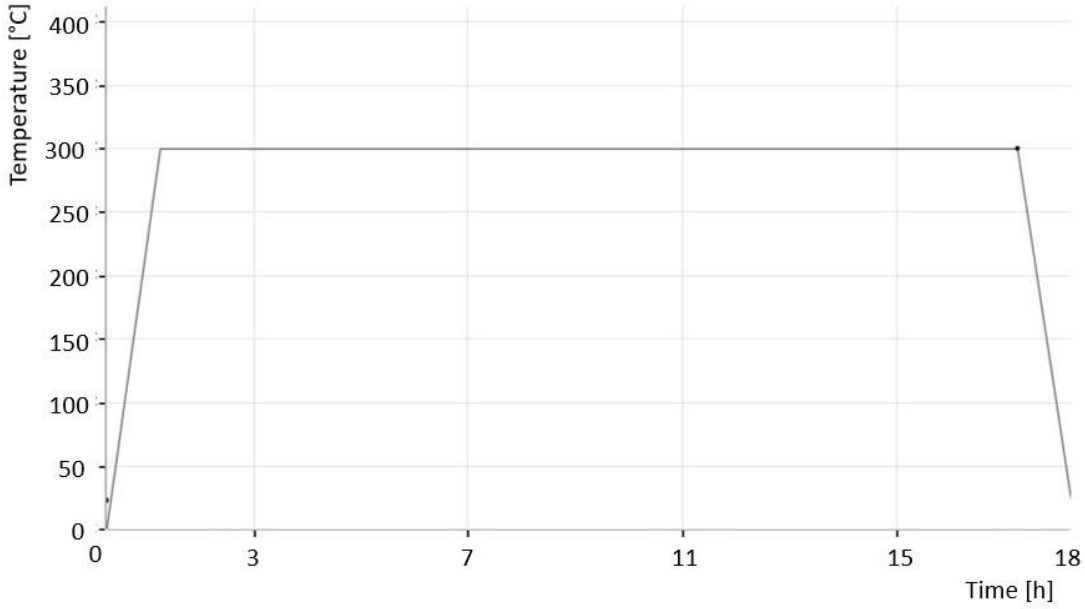

Figure 11 - Temperature ramp of thermal annealing treatment from Thermo Scientific software.

1.4 Photoluminescence measurements

Photoluminescence (PL) measurements were made using the Edinburgh Instruments FS5 Spectrofluorometer with a configuration allowing qualitative analysis only. The scheme of the spectrofluorometer is shown in Fig. 12.

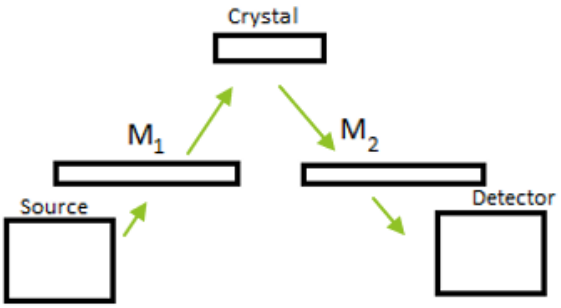

Figure 12 - Scheme of the spectrofluorometer.

A xenon lamp was the excitation source (230–1000 nm) and the excitation light was selected by the monochromator *M*1 while the light emitted (200-870 nm) by the sample passed across the monochromator *M*2 and was detected by a photomultiplier. Emission and excitation spectra were acquired by setting specific excitation/emission wavelength. FS5 advanced software enables two-dimensional excitation-emission maps acquisition. LYSO:Ce crystal on the sample holder is shown in Fig. 13.

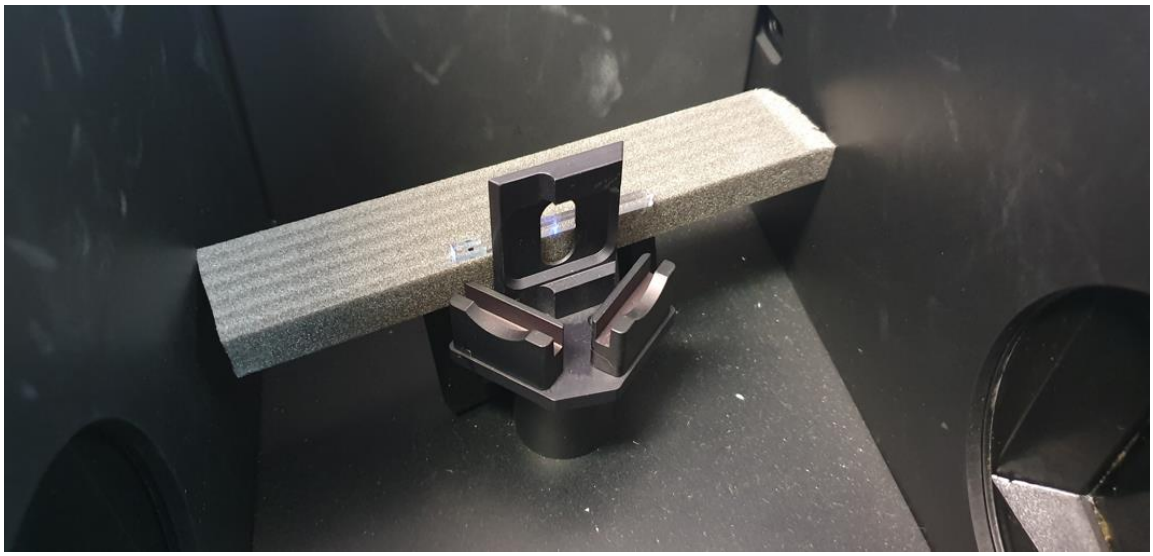

Figure 13 - FS5 customized sample holder compartment view**.**

2 Results and discussion

One of the key feature of LYSO:Ce crystals is the radiation resistance, since charged particles fluxes, relevant in high energy physics experiment, are responsible of the scintillator performance (transparency and light yield) losses.

The research activity of this work was focused on the analysis of LYSO:Ce crystals from 12 different vendors. Optical spectroscopy instrumentation was used to acquire transmission and emission spectra before and after irradiation and also after thermal treatment. In order to verify LYSO:Ce crystal bar radiation resistance, different samples were irradiated up to 50 kGy.

Longitudinal transmittance measurements (optical path d = 57 mm) were performed before irradiation for different samples of each vendor to verify the production quality. A comparison between each vendor was made through the average spectra. Furthermore, to investigate the cerium dopant presence, transversal transmittance measurements (optical path d = 3.75 mm) were acquired.

To quantify the transparency losses, the induced absorption coefficient μ was calculated for each irradiated sample at 420 nm. The μ coefficient is defined as:

$$\mu = \frac{1}{d}\ln\left(\frac{T_{before}}{T_{after}}\right) \tag{15}$$

where T_{before} and T_{after} are the sample transmittance values before and after irradiation.

The value at 420 nm was chosen because it corresponds to the maximum luminescence of the crystal when used as a scintillator as in our case. By definition (Beer-Lambert law), this coefficient is proportional to the density of absorption centres (colour centres) induced by ionizing radiation in the crystal [10].

Two-dimensional distribution of the UV-excitation and the PL spectra were also analysed for one crystal per vendor.

2.1 Transmittance measurements before irradiation

For this study, LYSO:Ce crystals with dimensions 57.0x3.12x3.75 mm were analysed. Longitudinal spectra were performed for each crystal available for each vendor as a function of the wavelength **λ** in the range 350 nm-650 nm with 2 nm steps. The transversal transmittance was measured in the range 330-380 nm with 2 nm steps.

2.1.1 Reproducibility of the measurement

Two reproducibility tests were performed for longitudinal transmittance measurements. In the first one, transmittance measurements were repeated without removing the crystal from the sample holder and acquired spectra are shown in Fig. 14.

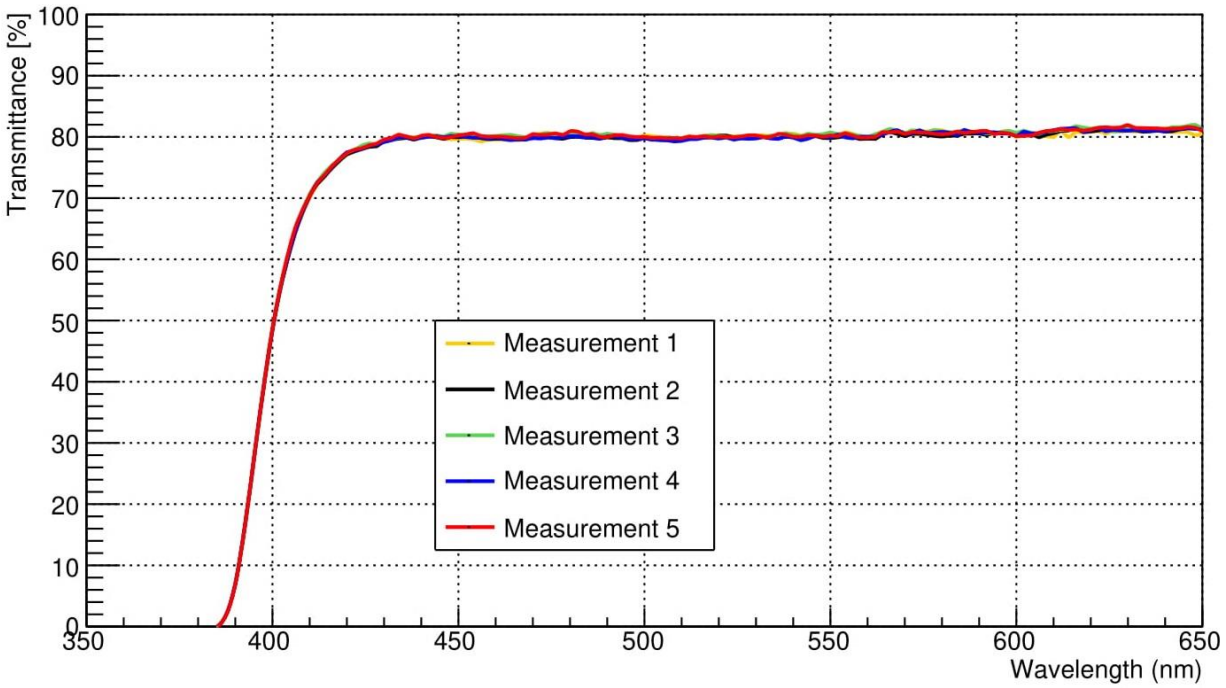

Figure 14 - Longitudinal measurements: 1^{st} reproducibility test.

The spread σ of %T values at each wavelength was calculated as:

$$\sigma = \frac{T_{max} - T_{min}}{2} \tag{16}$$

where T_{max} and T_{min} are the maximum and minimum transmittance value respectively of the set of measurements. The histogram shows that the maximum σ value for the first reproducibility test is σ = 0.7% (Fig. 15) and in average sigma is 0.2%.

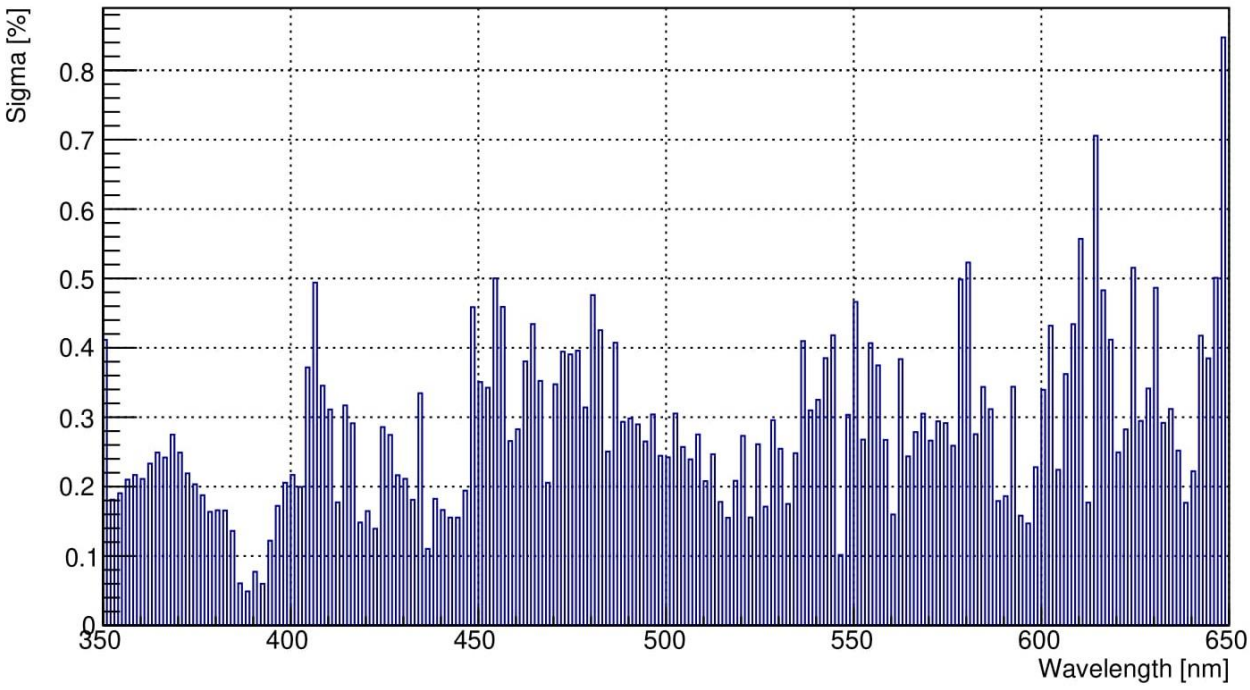

Figure 15 - Sigma σ value for longitudinal transmittance measurements, repeated without removing the crystal from the sample holder (1^{st} reproducibility test).

In the second reproducibility test the crystal was removed and relocated on the sample holder for each acquisition. Transmission spectra are reported in Fig. 16.

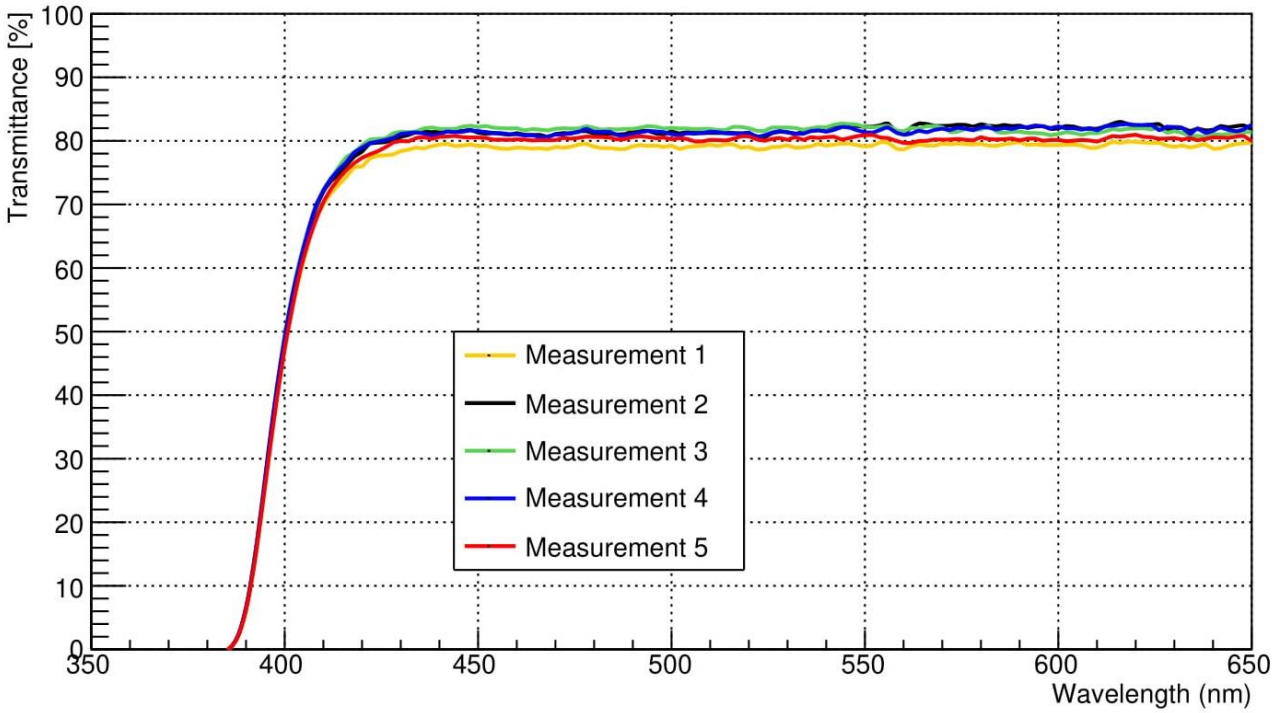

Figure 16 - Transmittance longitudinal measurements: 2^{nd} reproducibility test.

The σ value as a function of wavelength is shown in Fig. 17, in average sigma is 1.1%.

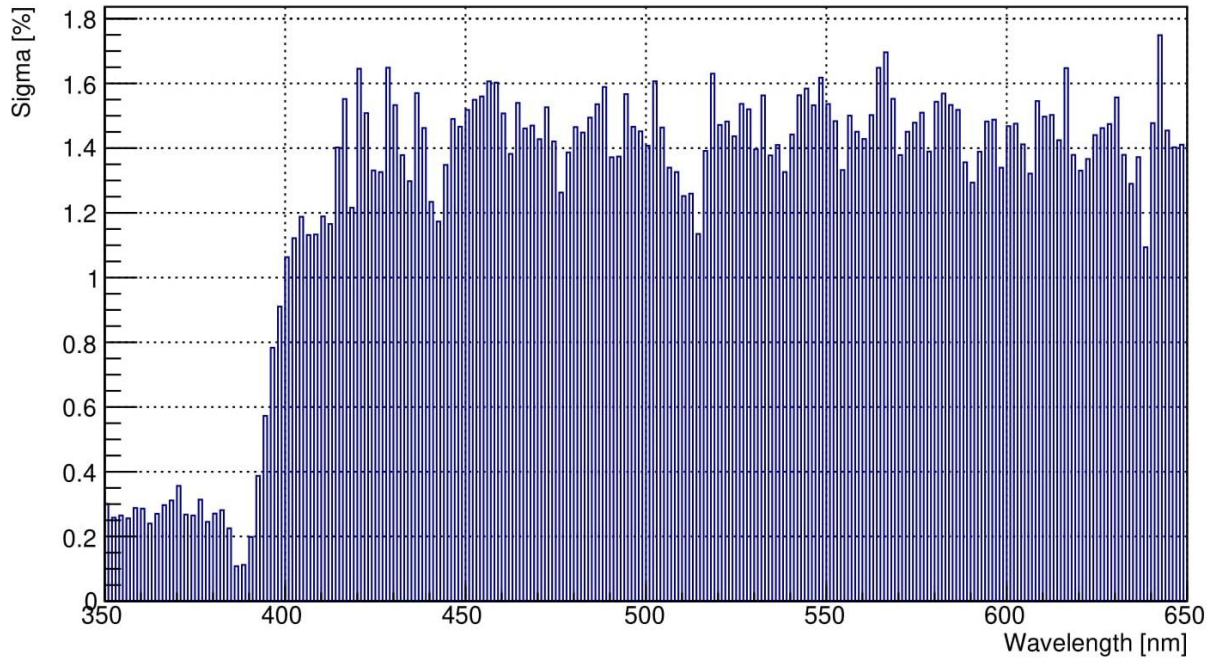

Figure 17 - Sigma σ values for repeated longitudinal transmittance measurements performed removing and replacing the crystal on the holder (2^{nd} reproducibility test).

Considering the first and the second reproducibility tests, a value of σ = 1.8% was chosen as longitudinal transmittance measurement uncertainty. To get an estimate of the Ce^{3+} concentration in the crystal, transversal transmission spectra were necessary because the large optical path in longitudinal measurements led to saturation of the instrument signal in the Ce^{3+} absorption region (around 355 nm). As well known, the position of the energetic levels of free Ce^{3+} are strongly modified in the presence of the crystal field [13]] and, in the case of LYSO:Ce crystal, the absorption lines corresponding to F-D transitions are shifted in the near UV.

2.1.2 Longitudinal transmittance measurements

A number from 1 to 12, was assigned randomly to producers reported at the beginning of Chapter 2. In the following, crystals will be identified by the producer ID (e.g. P05) and by the crystal BarCode (e.g. BC075). Longitudinal transmission spectra of different crystals from the same vendor, were compared to quantify the transmittance homogeneity within each producer. Crystals from the same vendor are expected to have a similar transmittance. Transmission spectra of the analysed crystals from producer P07, are reported in Fig. 18, as an example. Afterwards, an average spectrum was obtained for each vendor.
In order to characterize the optical transmission, a quantity called λ_{cutoff} is introduced. It is defined as the wavelength value at which the linear fit of the optical absorption edge crosses the x-axis (%T = 0), as shown in Fig. 19.

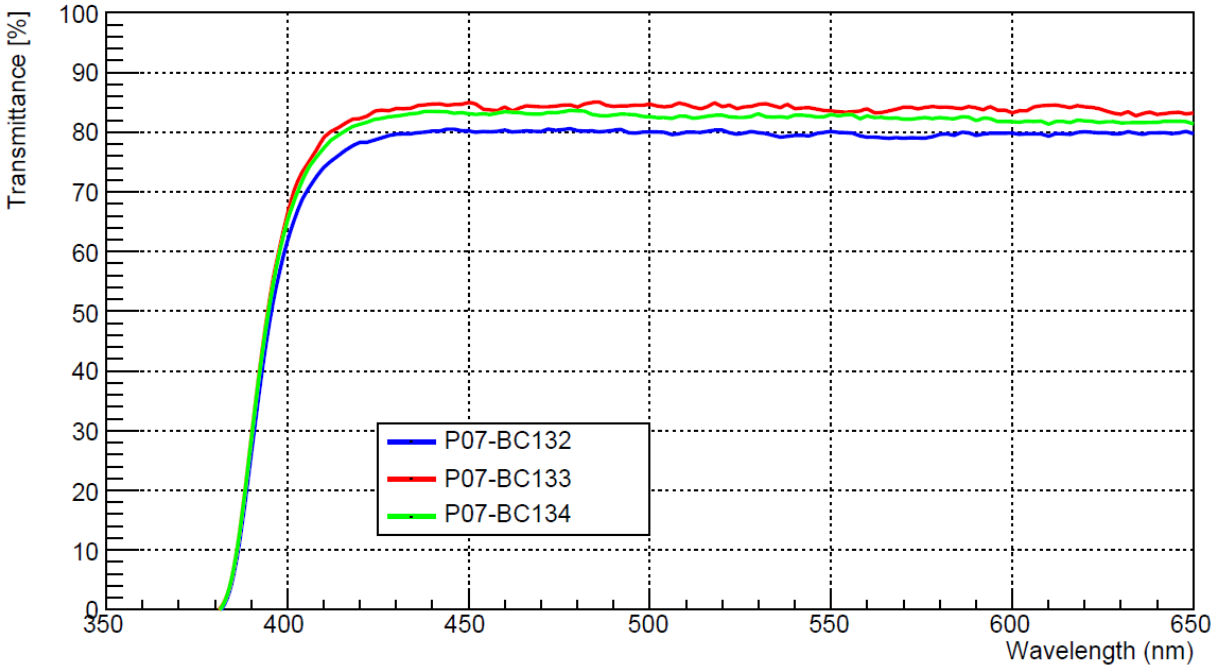

Figure 18 - Transmission spectra of three different crystals from vendor P07.

The transmittance values at **λ** = 396 nm and **λ** = 420 nm, were also chosen as qualifying parameters, as will be illustrated in the following, because they correspond to the maximum values of LYSO:Ce emission spectrum.

Transmittance values at **λ** = 600 nm were also considered. Indeed, in this region, it is possible to calculate the theoretical limit of the transmittance considering no internal absorption, as shown in the following.
Crystals from the same vendor show a slightly different percentage of transmittance but they all have the same λ_{cutoff}.

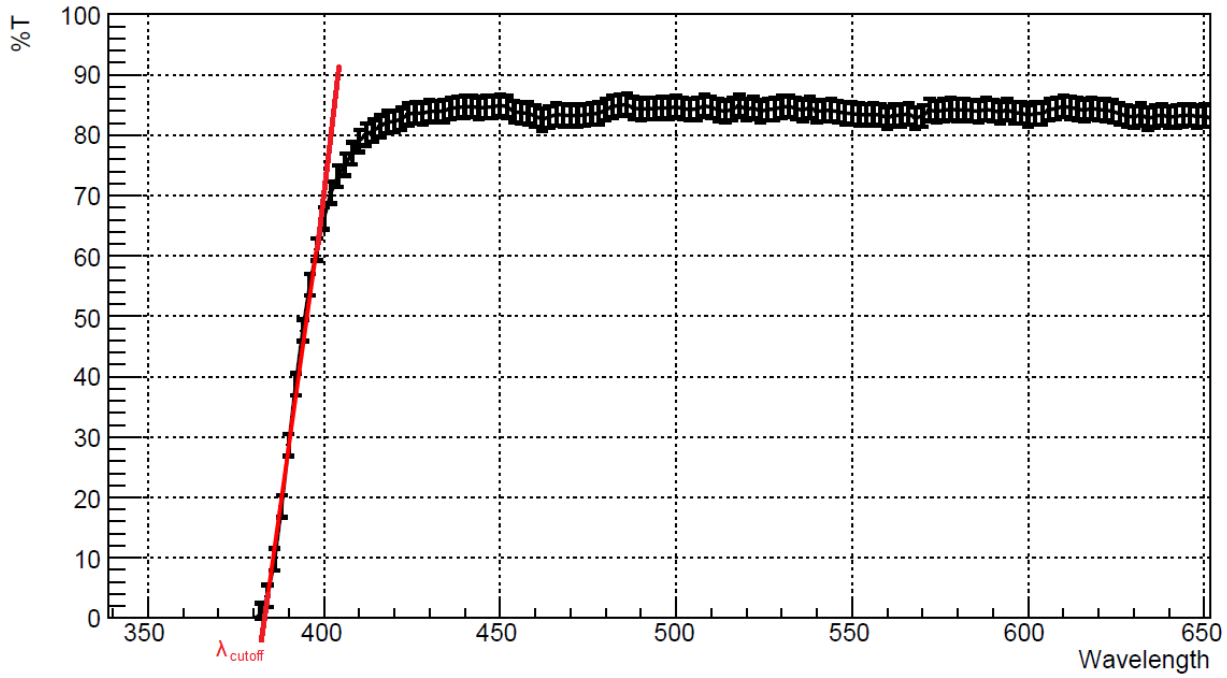

Figure 19 - P07-BC133 crystal longitudinal transmission spectrum. λ_{cutoff} is defined as the wavelength value at which the linear fit of the absorption edge (red line) crosses the x-axis.

The obtained average transmission spectra of each vendor are shown in Fig. 20 and the corresponding parameters are reported in Table 1. In the first three columns, the percentage transmittance values are referred to the average spectra. In the last column, the number inside parenthesis is the number of crystals used to calculate the mean value while the percentage is the transmittance maximum semi-dispersion at 420 nm. Vendors from P04 to P09 have a transmittance spread higher than the measurement error while the other seem to have a better production quality.

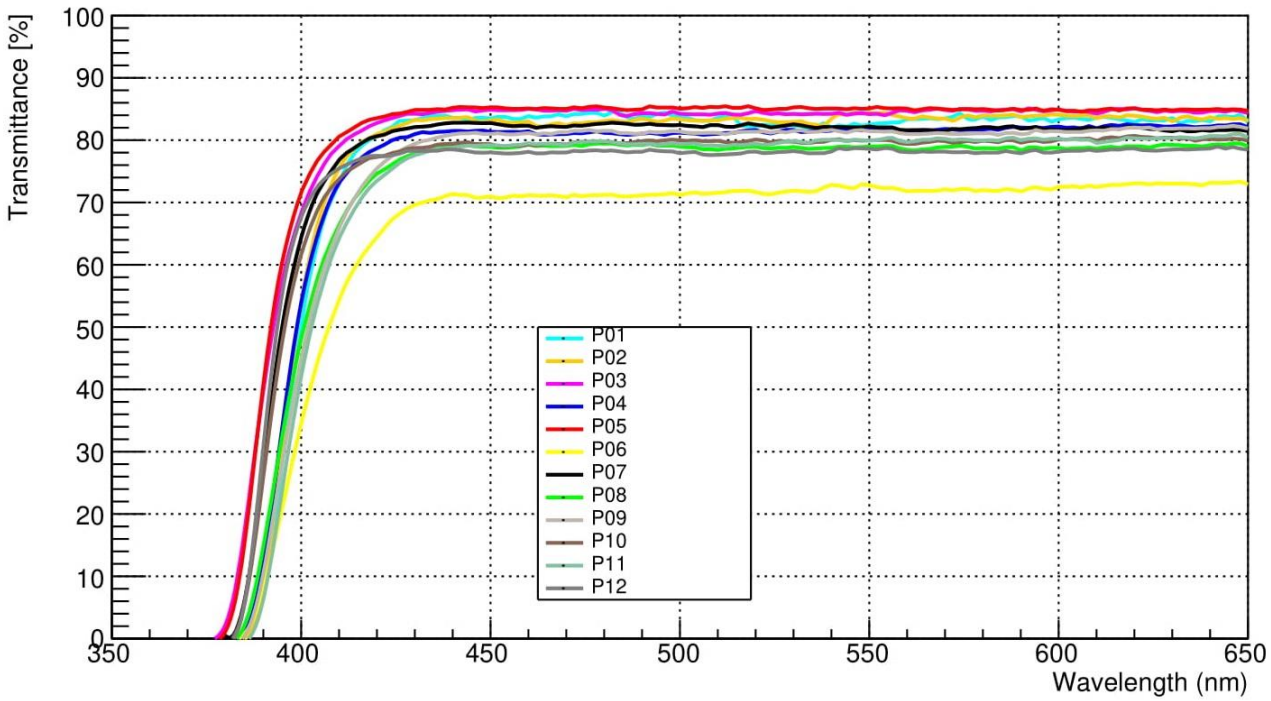

Figure 20 - Average longitudinal transmission spectra of crystals of different vendors.

Table 1 - Average transmission spectrum parameters of samples from different vendors. λ_{cutoff} error is 1 nm, %T error is 1.8.

Vendor	**%T (396 nm)**	**%T (420 nm)**	**%T (600 nm)**	$\boldsymbol{\lambda_{cutoff}}$	$\boldsymbol{\Delta T_{MAX}}$ **(420 nm)**
P01	32.9	80.0	83.4	387	0.8%
P02	36.6	81.0	84.1	387	0.5%
P03	59.8	81.7	84.5	380	1.1%
P04	38.5	78.7	81.2	386	2.2%
P05	63.2	83.5	84.9	380	1.9%
P06	23.7	64.4	72.5	386	3.1%
P07	53.7	80.6	81.6	383	2.0%
P08	36.0	74.6	78.8	385	2.7%
P09	31.9	75.5	81.4	386	5.3%
P10	51.2	77.3	80.1	383	0.4%
P11	27.9	73.5	80.3	388	0.1%
P12	58.9	77.5	78.2	384	0.3%

Furthermore, the average transmittance value at 420 nm for each producer is reported in Fig. 21.

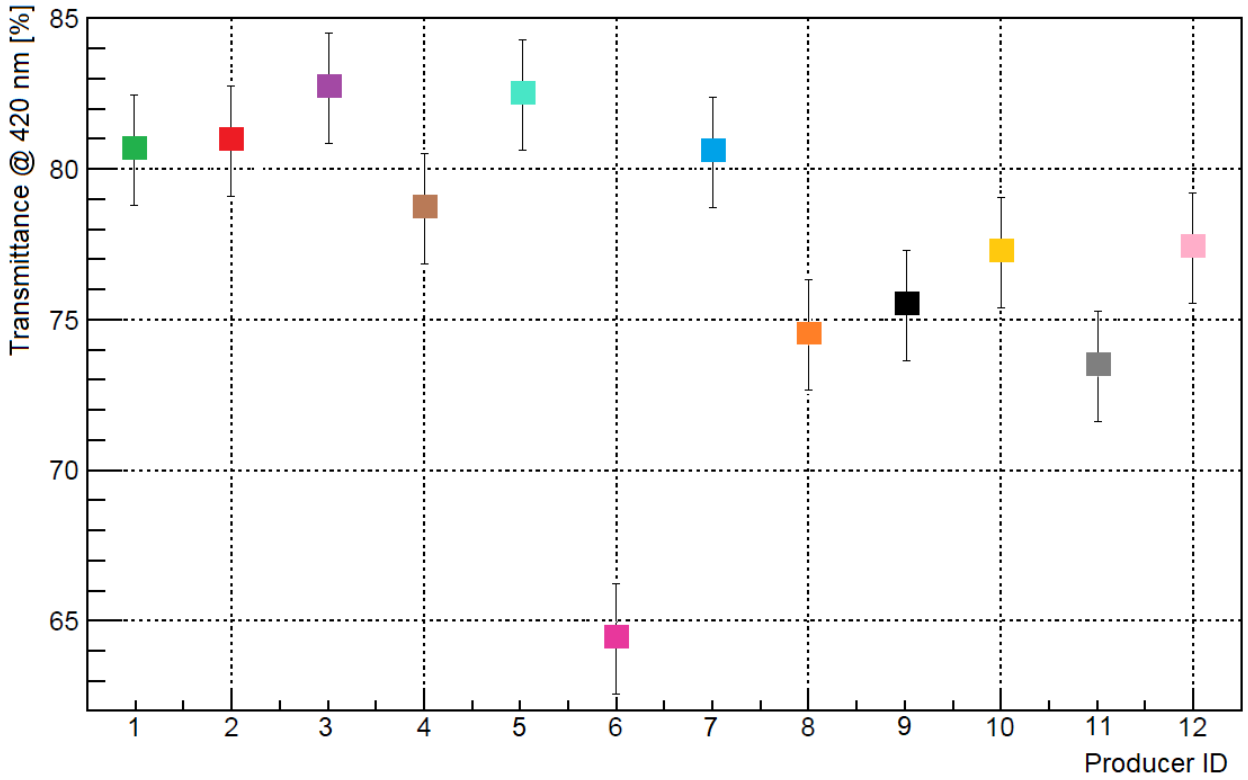

Figure 21 - Average transmittance values at 420 nm of crystals of different vendors.

The crystal from P06 vendor has T(420 nm) < 65% while most of the vendors have T(420 nm) > 75% and five of them have T(420 nm) > 80%. The vendor P06 crystals, in fact, appear translucent at a naked eye (visual inspection), as illustrated in Fig. 22.

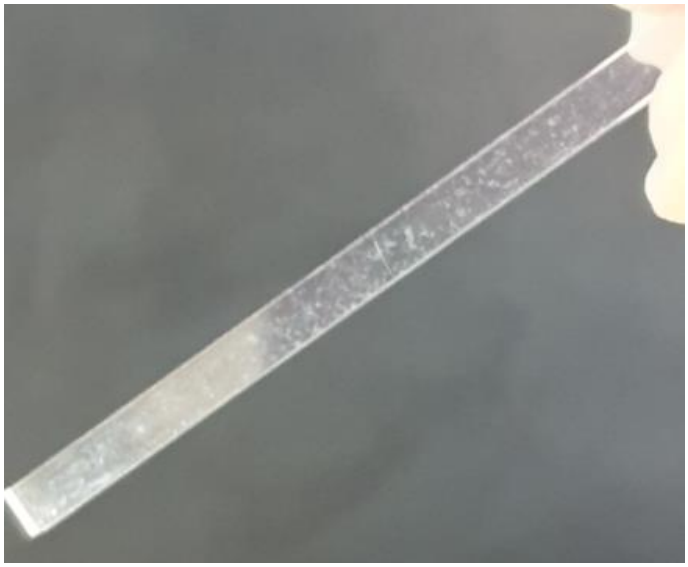

Figure 22 - One of the P06 crystals.

Assuming null internal absorption of the light, the expected transmittance, for a crystal of thickness *d*, is [14] [15]:

$$T = \frac{1 - R(\lambda)}{1 + R(\lambda)} \tag{17}$$

where R is the reflectivity which depends on the wavelength value according to:

$$R(\lambda) = \frac{[n(\lambda)_{crystal} - n(\lambda)_{air}]^2}{[n(\lambda)_{crystal} + n(\lambda)_{air}]^2} \tag{18}$$

where $n(\lambda)_{crystal}$ is the LYSO:Ce refractive index at the wavelength λ and $n(\lambda)_{air}$ is the air one. For wavelengths in the range 405-546 nm, the refractive index values (Tab. 2) were calculated [14] and used to obtain the percentage of transmittance according to Formula 17. The transmittance values corresponding to the wavelengths.

Table 2 - LYSO:Ce refractive indexes. The error on the refractive index values is 0.001 [14].

Wavelength [nm]	Refractive index
405	1.833
420	1.827
436	1.822
461	1.818
486	1.813
516	1.810
546	1.806

reported in Tab. 2, are shown in Fig. 23 together with the average transmission spectrum of crystals from vendor P04 (T(600 nm) > 80%).

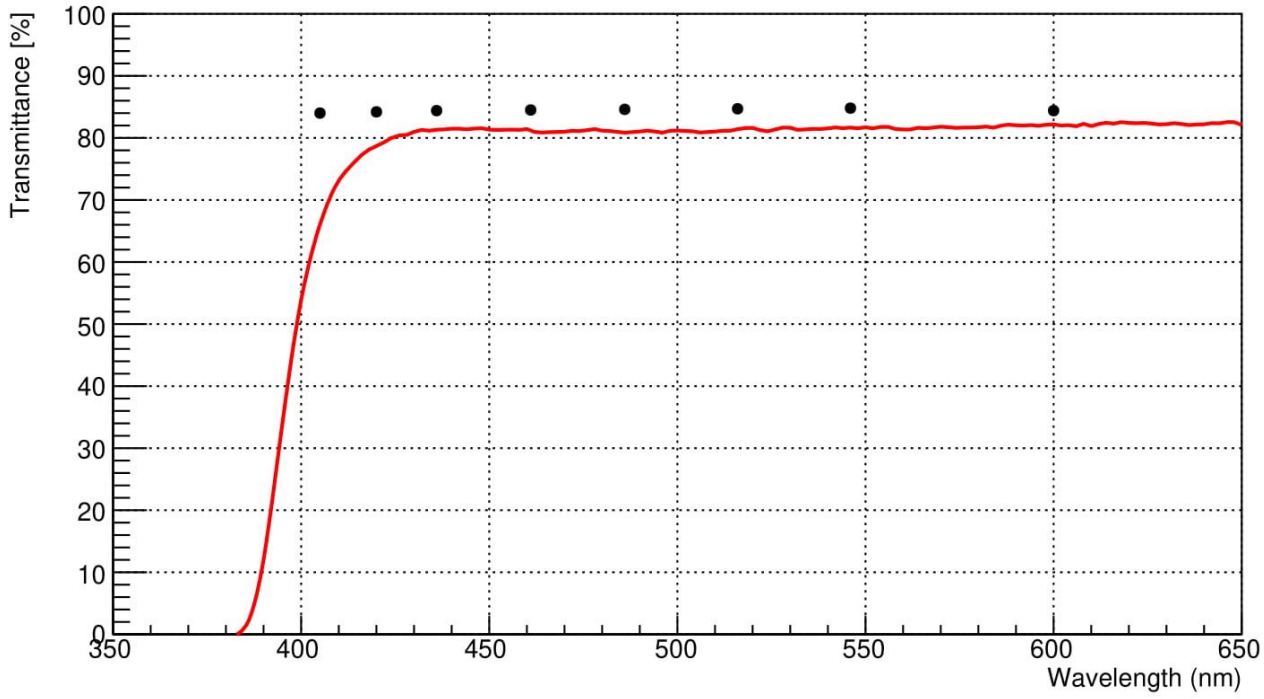

Figure 23 - Average transmission spectrum of crystals from vendor P04. The black dots represent the calculated theoretical limit of transmittance.

Therefore, all vendors are characterized by a reduced transmittance with respect to the theoretical limit. This is possibly due to not perfectly parallel faces and to small effects of internal absorption.

2.1.3 Transversal measurements and Ce^{3+} peak study

Transversal transmittance measurements were acquired in order to investigate the cerium peak in the UV range. The cerium ions in LYSO:Ce matrix are found both in Ce^{3+} and Ce^{4+} states. The absorption peak analyzed in this work is the Ce^{3+} one, it is positioned in the range 350-360 nm as shown in Fig. 24 where transversal transmission spectra are reported for each vendor.

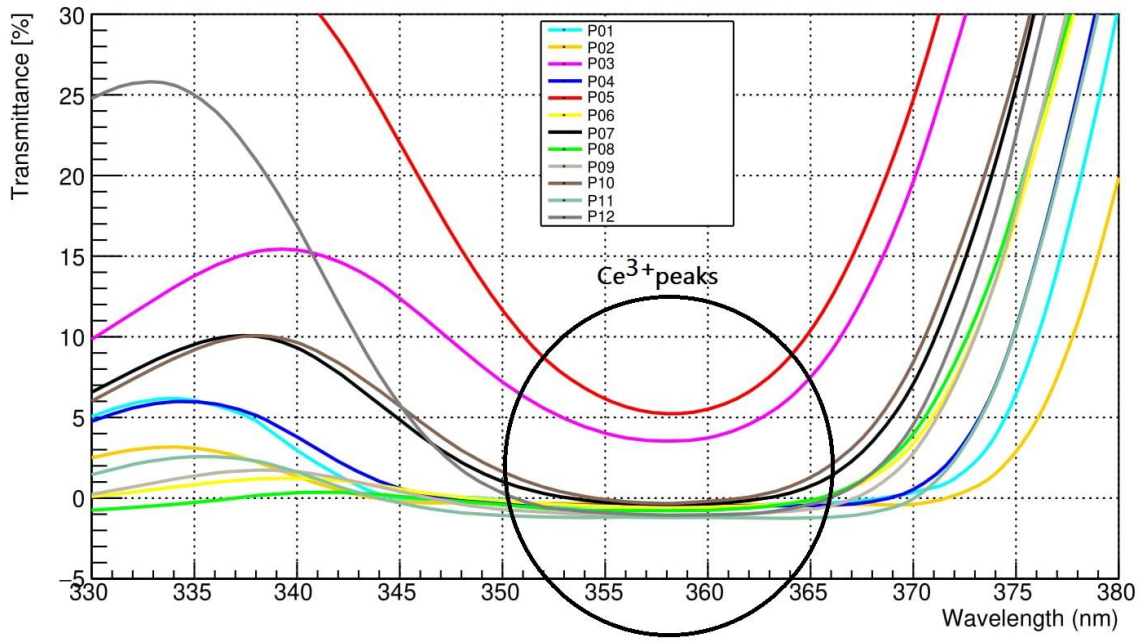

Figure 24 - Transversal transmission spectra for each vendor.

Only for vendors P03 and P05 the transmission spectrum can be converted into an absorbance one, as shown in Fig. 25 as an example for vendor P05, through the formula:

$$A = Log\left(\frac{1}{T}\right) \tag{19}$$

where A is the absorbance, T the transmittance and Log represents the logarithm with base 10.

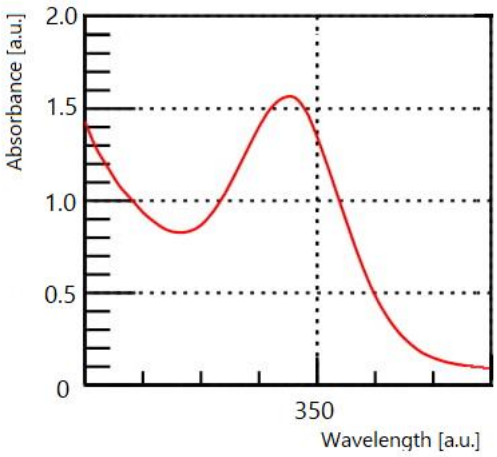

Figure 25 - Absorbance peak for vendors P05.

For the other vendors, the transmittance vanishes in the range between 355 nm and 360 nm, i.e. the crystals absorb all the light in this range and the absorbance is infinity. The cerium concentration will be discussed in Section 3.4, taking into account the absorbance peak and the damages after irradiation.

2.2 Photoluminescence measurements before irradiation

Unlike the scintillation (radio-luminescence) process where the excitation of the luminescent centre occurs following the deposit of energy by an ionizing radiation, in photoluminescence (PL) the excitation is due to the absorption of photons from a source of light. Photoluminescence measurements are a very useful tool for the study of luminescence centres involved in the scintillation process.

PL measurements were performed for crystals of different vendors. The excitation spectra were acquired in the range 240-390 nm with a constant emission wavelength $\lambda_{em} = 420\, nm$. The emission spectra were recorded in the range 370-550 nm by exciting the crystals with $\lambda_{ex} = 358\, nm$. The values $\lambda_{ex} = 358\, nm$ and $\lambda_{em} = 420\, nm$ correspond to the maximum of the excitation and emission spectra, respectively, for each vendor. All measurements were performed with 2 nm steps.

2.2.1 Reproducibility of the measurement

A reproducibility test was performed for emission measurements by removing and replacing the crystal on the holder for each measurement. The resulting emission spectra ($\lambda_{ex} = 358\, nm$) are shown in Fig. 26.

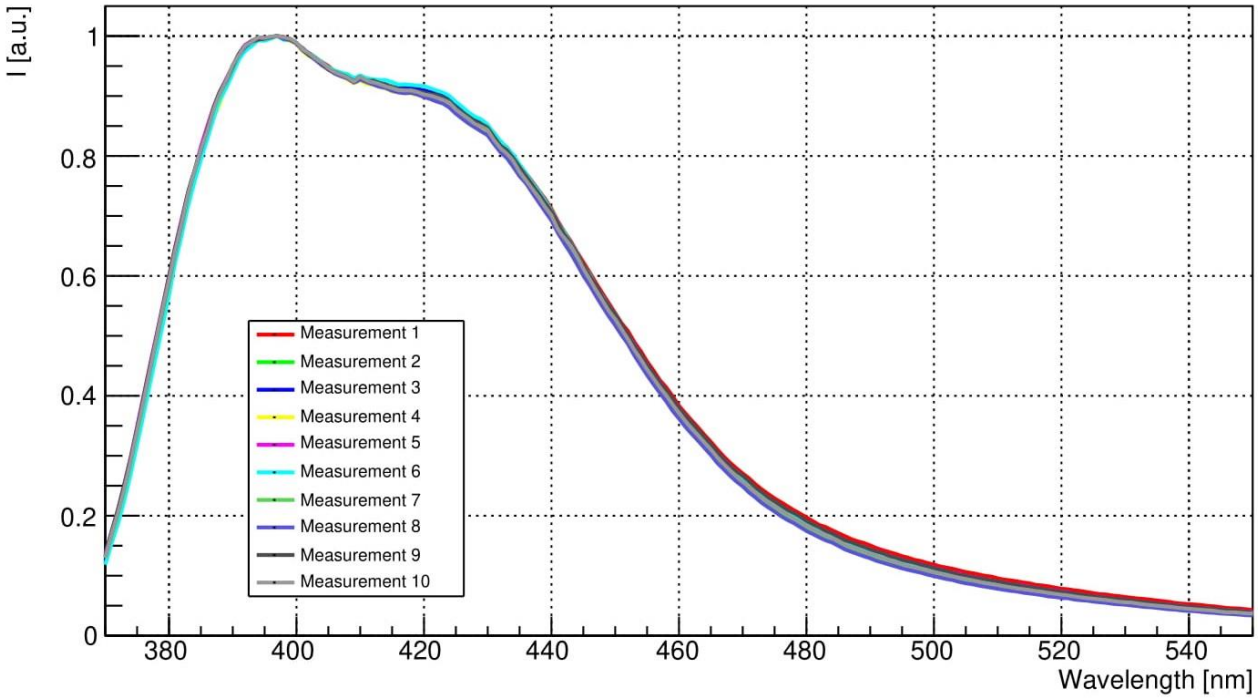

Figure 26 - Emission spectra reproducibility test.

Each spectrum is normalized at its maximum intensity value. In order to evaluate the measurements dispersion, a simple measure of spread was made. The spread σ of the emission intensity, obtained with the Formula 16, is in average $\sigma \sim 0.9\%$ and it never exceeds the value $\sigma \sim 1.6\%$.

2.2.2 Emission and excitation spectra

The emission spectra for different vendors, normalized at the maximum intensity value, are shown in Fig. 27.

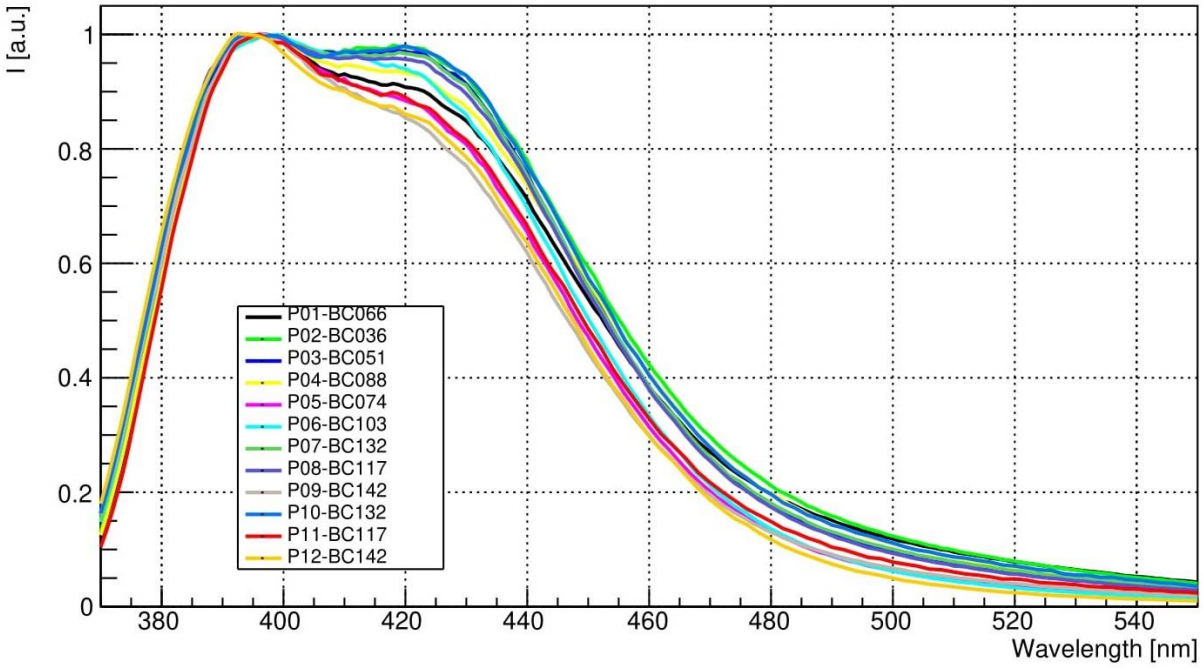

Figure 27 - Emission spectra for different vendors crystals ($\lambda_{ex} = 358\ nm$).

The position corresponding to the maximum value of the emission spectra is the same for all the vendors, while the relative intensity percentage ratio at $\lambda_{em} = 420\ nm$ with respect to $\lambda_{em} = 396\ nm$ is slightly different. In Table 3 the relative intensity for each vendor is reported.

Table 3 - Emission relative intensity at $\lambda_{em} = 420\ nm$.

Vendor	**Intensity ratio** $\frac{I_{420\ nm}}{I_{396\ nm}}$
P01	0.98
P02	0.98
P03	0.97
P04	0.93
P05	0.88
P06	0.94
P07	0.97
P08	0.96
P09	0.85
P10	0.98
P11	0.89
P12	0.86

The LYSO:Ce excitation spectrum (red curve in Fig. 28) shows three peaks, corresponding to the excitation wavelengths at which the maximum emission occurs. The difference between the wavelengths of the emission spectrum peak and the excitation spectrum peak, is called Stokes shift. When an atom absorbs a photon, one of its electrons moves to a higher electronic state; the atom de-excites emitting a lower energy photon, as the electron returns to a lower energy state.

In Fig. 28, emission and excitation spectra are shown together with the transmission spectra, for P01-BC066 crystal, as an example.

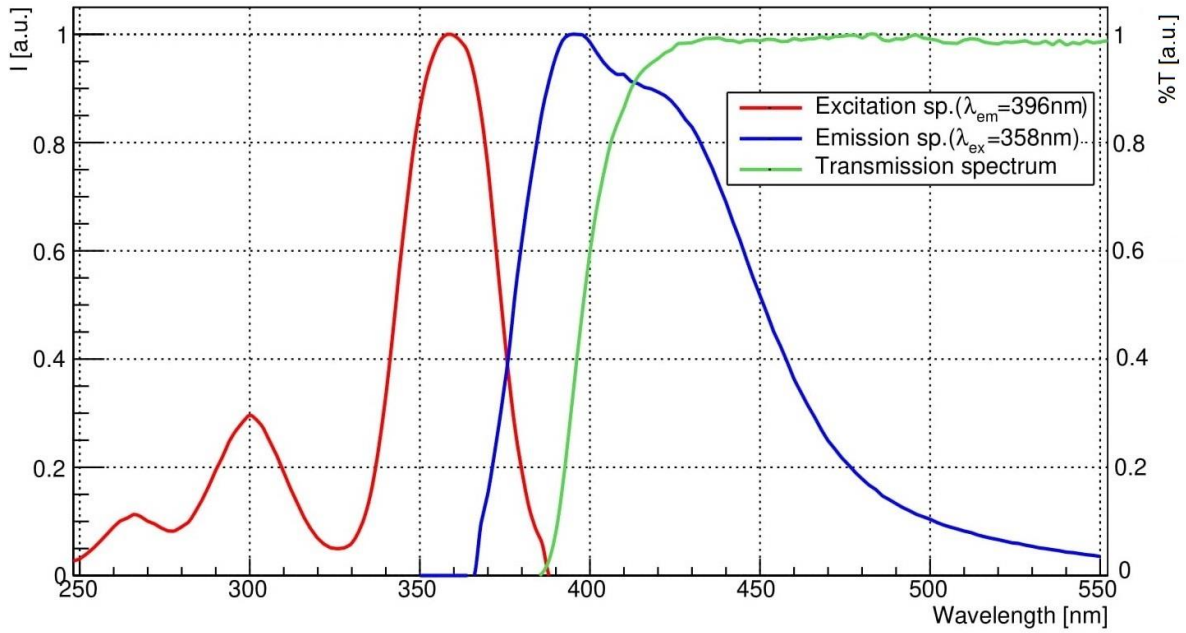

Figure 28 - P01-BC066 excitation (red), emission (blue) and transmission (green) spectra as a function of the wavelength.

The most intense peak of the emission spectrum is the one at 396 nm but at this wavelength, due to the absorption edge of the transmission spectrum (at around 390 nm), the emitted light is partially reabsorbed by the crystal [14][16][17]. Therefore, only the peak at 420 nm will be considered in the following discussion. The emission spectrum weighted for the transmittance, is shown in Fig. 29 for P01-BC066, as an example.

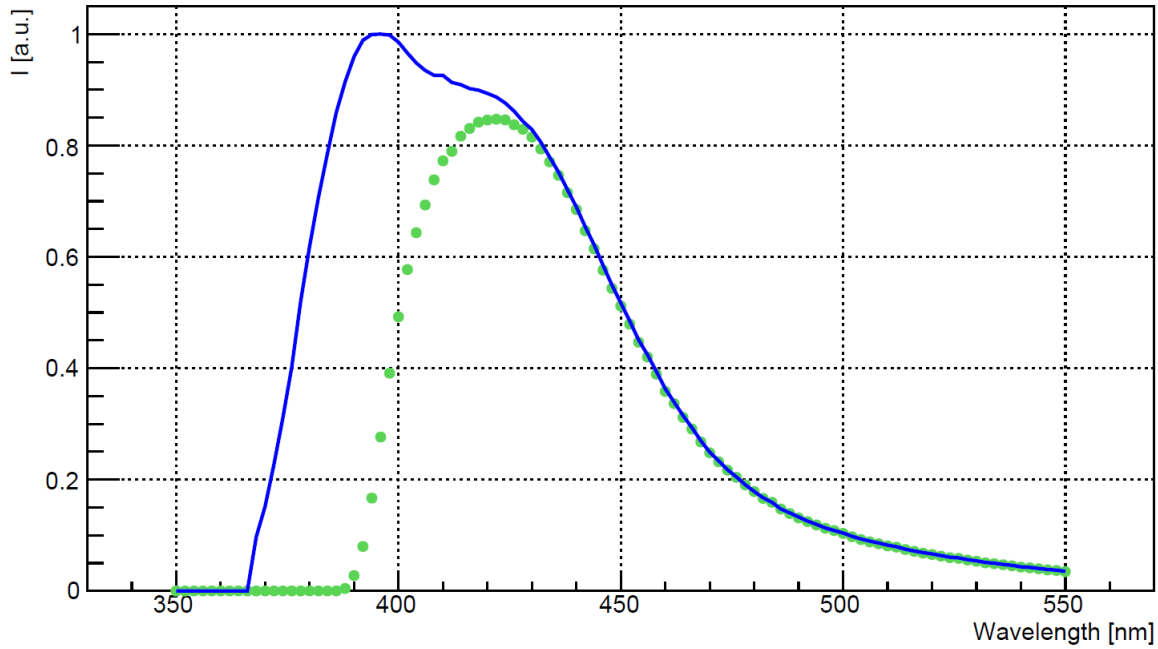

Figure 29 - P01-BC066 emission spectrum weighted for the transmittance (green dots) and emission spectrum (blue curve).

The resulting LYSO:Ce emission spectrum is almost completely detected by a light detector such as the SiPM, as can be seen from its photon detection efficiency curve reported in Fig. 30. Moreover higher $\frac{I_{420\,nm}}{I_{396\,nm}}$ ratio is preferable to achieve better light collection.

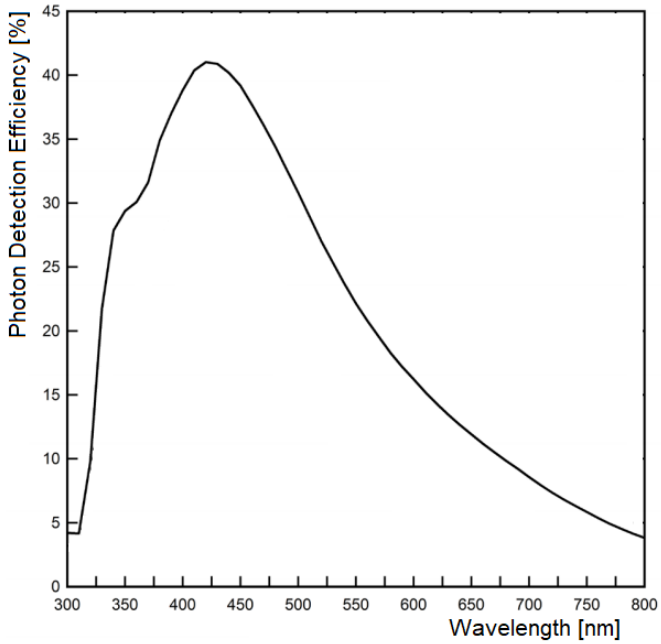

Figure 30 - Photon detection efficiency curve of the SiPM.

2.2.3 Emission maps

A two-dimensional map of the UV-excitation (240-390 nm) and emission spectra (350-550 nm) was produced with the FS5 Spectrofluorometer (Fig. 31).

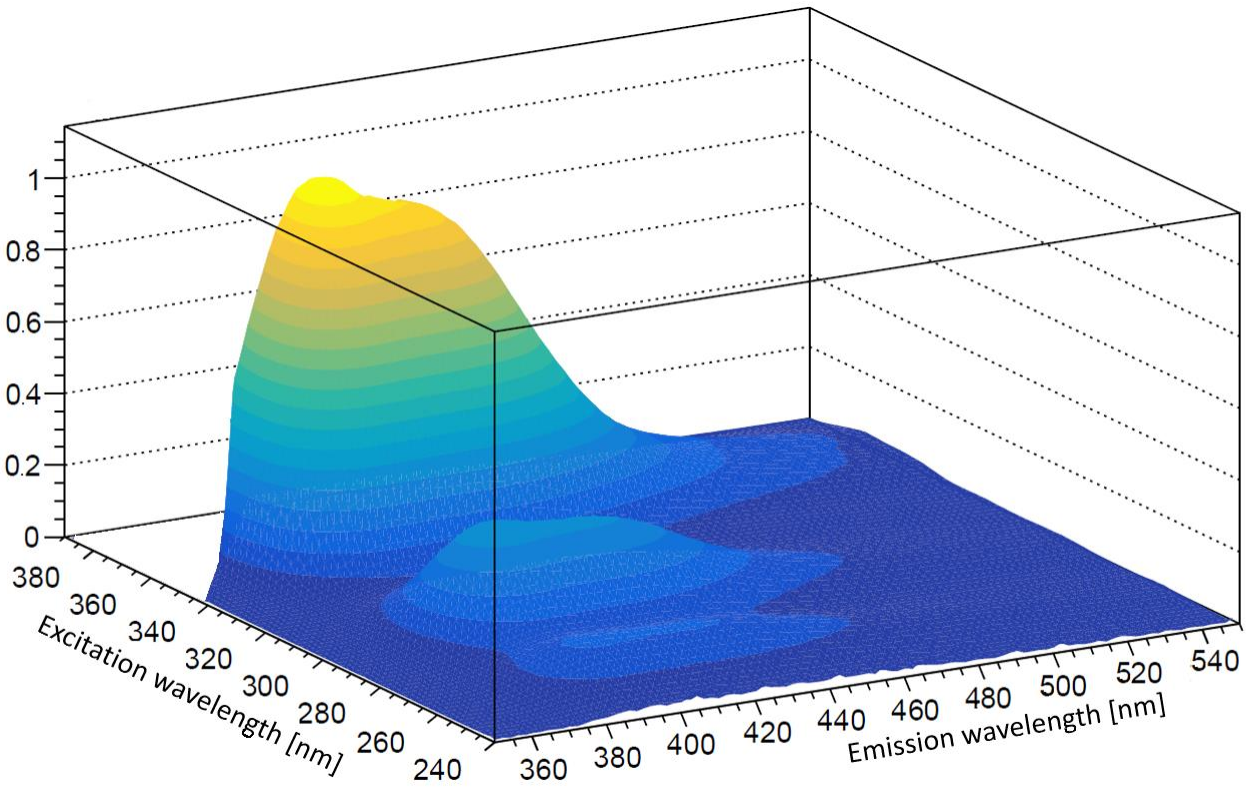

Figure 31 - P01-BC066 three-dimensional plot of the UV-excitation and emission spectra.

The maximum corresponds to $\lambda_{em} = 396\,nm$ and $\lambda_{ex} = 358\,nm$.

The absolute maximum is at $\lambda_{em} = 396\,nm$ and $\lambda_{ex} = 358\,nm$.
In order to avoid the excitation light of the spectrofluorometer, entering the detector, it was not possible to acquire the whole excitation and emission ranges (white triangle in Fig. 31) and the data were acquired with the constraint: $\lambda_{em} > \lambda_{ex}$.

2.3 Irradiation tests

The irradiation tests were performed on samples from different vendors. Some crystals were irradiated up to 50 kGy at the maximum available dose rate (7.87 kGy/h) at Calliope facility (Section 2.2). In order to investigate the effects of thermal treatment on their optical properties, some of them were annealed at 300 °C for 16 hours, as summarized in Tab. 4. In particular, the thermal annealing was performed to study the recovery of the radio-induced defects. For one sample (P05-BC076) the same treatment was carried out before the irradiation test to investigate the effect of thermal annealing on the crystal radiation resistance [18].
The crystals were kept in the dark at room temperature during and after the irradiation test and several measurements were performed in time to evaluate the possible dark recovery.

Table 4 - Summary of treated crystals.

Crystal	Thermal Annealing	Absorbed dose [kGy]	Total absorbed dose [kGy]
P01-BC031	After irradiation	50	50
P02-BC037	After irradiation	50	50
P03-BC052	After irradiation	50	50
P05-BC074	/	43	43
P05-BC075	After irradiation	38 + 12	50
P05-BC076	Before irradiation	43	43
P07-BC133	After irradiation	38 + 12	50
P09-BC143	After irradiation	38 + 12	50

2.3.1 Transmittance measurements after irradiation

P01-BC031, P02-BC037 and P03-BC052 crystals were irradiated at 50 kGy in a single step and the transmittance curve of crystal P02-BC037 is shown in Fig. 32 as an example. Comparing the %T curves, it is evident a slight red shift and a decrease of transmittance in the whole range induced by gamma radiation. The other two analysed samples, P01-BC031 and P03-BC052, show the same behaviour. The parameters characterizing the spectra before and after irradiation for analysed crystals are reported in Tab. 5.

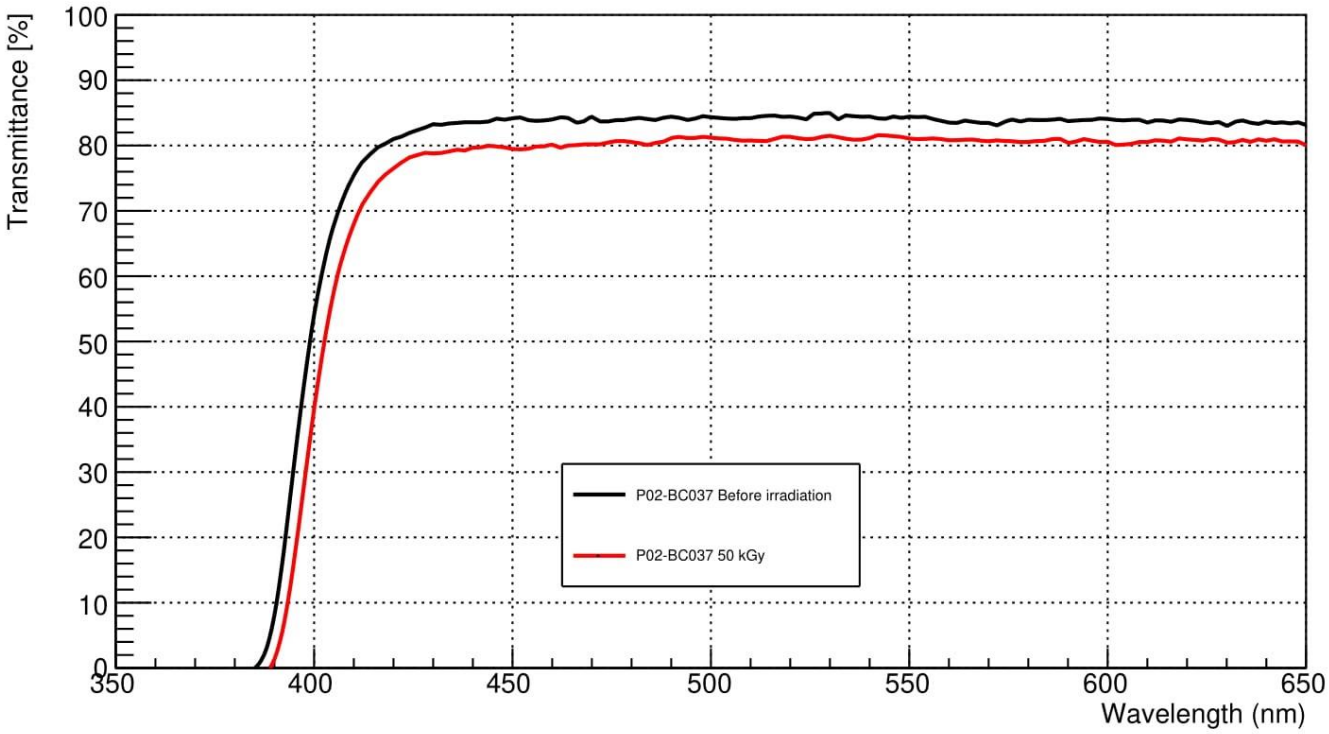

Figure 32 - Longitudinal transmission spectra before and after irradiation of crystal P02-BC037.

Table 5 - Transmission spectrum parameters of crystals from vendors P01, P02 and P03 before and after irradiation at 50 kGy. λ_{cutoff} error is 1 nm, %T error is 1.8.

P01-BC031	$\boldsymbol{\lambda_{cutoff}}$	**%T (420 nm)**	**T (600 nm)**
Before irradiation	387	79.2	82.2
After irradiation (50 kGy)	391	73.7	79.2
P02-BC037	$\boldsymbol{\lambda_{cutoff}}$	**%T (420 nm)**	**T (600 nm)**
Before irradiation	387	81.5	84.2
After irradiation (50 kGy)	391	76.5	80.6
P03-BC052	$\boldsymbol{\lambda_{cutoff}}$	**%T (420 nm)**	**T (600 nm)**
Before irradiation	379	82.8	84.9
After irradiation (50 kGy)	383	65.1	70.4

The P03 crystal seems to be more damaged, in term of transmission, after irradiation.

A second set of samples (P05-BC075, P07-BC133 and P09-BC143) were irradiated at 38 kGy (first step) and then up to 50 kGy (second step). Crystal from vendor P07 and P09 show a similar behaviour since after a worsening of transmittance after the first irradiation step, further significant %T losses were not measured at higher absorbed dose (Tab. 6).

Table 6 - Transmission spectrum parameters of crystals from vendors P05, P07 and P09 before and after irradiation at 38 kGy and 50 kGy. λ_{cutoff} error is 1 nm, %T error is 1.8.

P05-BC075	$\boldsymbol{\lambda_{cutoff}}$	**%T (420 nm)**	**T (600 nm)**
Before irradiation	380	85.7	86.9
After irradiation (38 kGy)	382	75.7	78.2
After irradiation (50 kGy)	383	68.1	70.1
P07-BC133	$\boldsymbol{\lambda_{cutoff}}$	**%T (420 nm)**	**T (600 nm)**
Before irradiation	383	82.3	83.3
After irradiation (38 kGy)	385	77.5	80.9
After irradiation (50 kGy)	385	74.5	77.6
P09-BC143	$\boldsymbol{\lambda_{cutoff}}$	**%T (420 nm)**	**T (600 nm)**
Before irradiation	386	81.6	86.4
After irradiation (38 kGy)	389	70.6	80.0
After irradiation (50 kGy)	390	69.9	76.5

Differently a remarkable optical degradation, with the increase of absorbed dose, characterizes sample from vendor P05, as shown in Fig. 33 and in Tab. 6. As for the first set of samples, the transmittance curve were shifted to longer wavelengths, with a maximum value of 4 nm for samples P05-BC075 and P09-BC143.

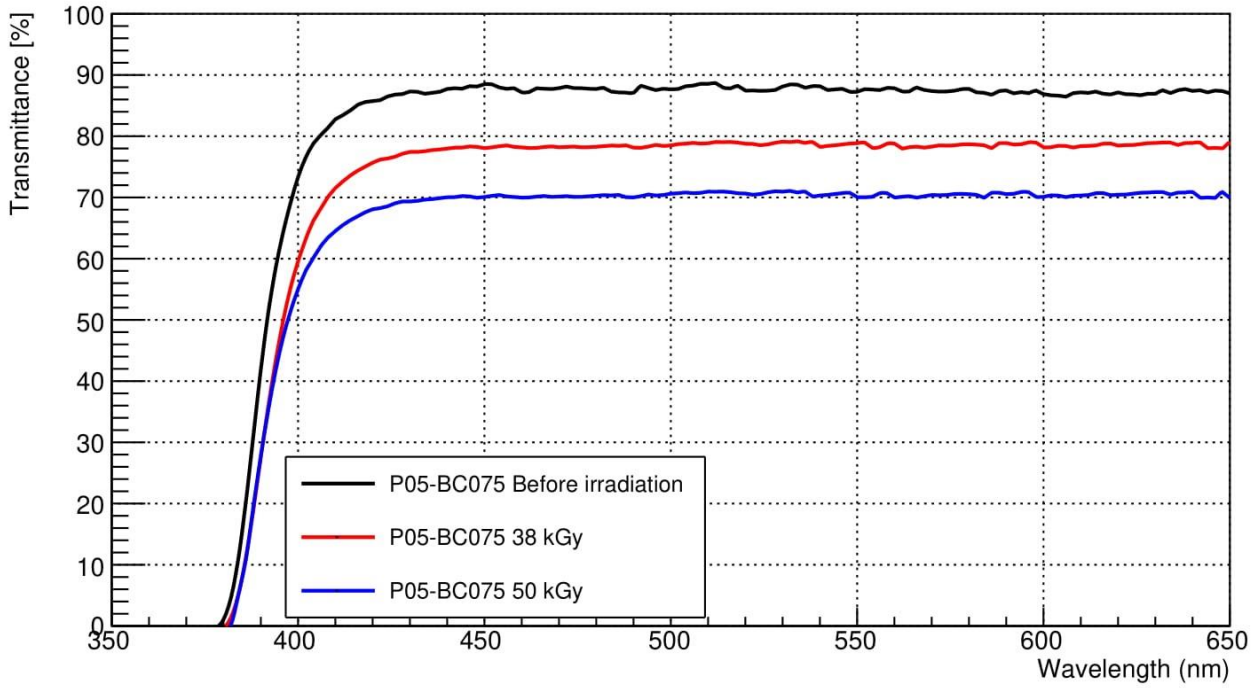

Figure 33 - P05-BC075 longitudinal transmission spectra before (black curve) and after irradiation at 38 kGy (red curve) and at 50 kGy (blue curve).

Radiation damage of the crystals was generally characterized by the radiation induced absorption coefficient μ (as defined at the beginning of this chapter), which depends on the colour centres density inside the crystal matrix. In the analysed LYSO:Ce crystals, the μ decreases monotonically with the wavelength [7], as shown in Fig. 34 for P05-BC075 crystal. In the same figure, it is evident the increase of damaging as a function of the absorbed dose.

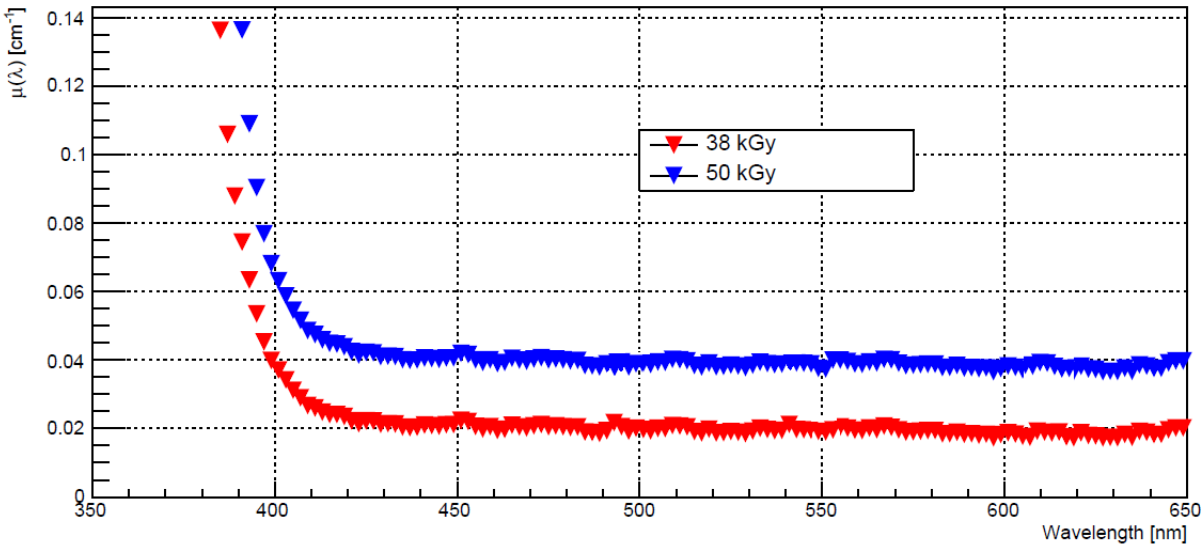

Figure 34 - Radiation-induced absorption coefficient μ, as a function of the wavelength, for P05-BC075 crystal at 38 kGy (red curve) and at 50 kGy (blue curve).

The radiation-induced absorption coefficient values at 420 nm are reported in Tab. 7 and a comparison of μ for each irradiated sample, at 420 nm for 50 kGy absorbed dose, is shown in Fig. 35.

Table 7 - Induced absorption coefficient μ for each irradiated crystal at 420 nm.

Crystal	μ (420 nm) at 38 kGy [cm^{-1}]	μ (420 nm) at 50 kGy [cm^{-1}]
P01-BC031	/	0.013±0.003
P02-BC037	/	0.011±0.003
P03-BC052	/	0.042±0.003
P05-BC075	0.022±0.003	0.040±0.003
P07-BC133	0.011±0.003	0.017±0.003
P09-BC143	0.025±0.003	0.027±0.003

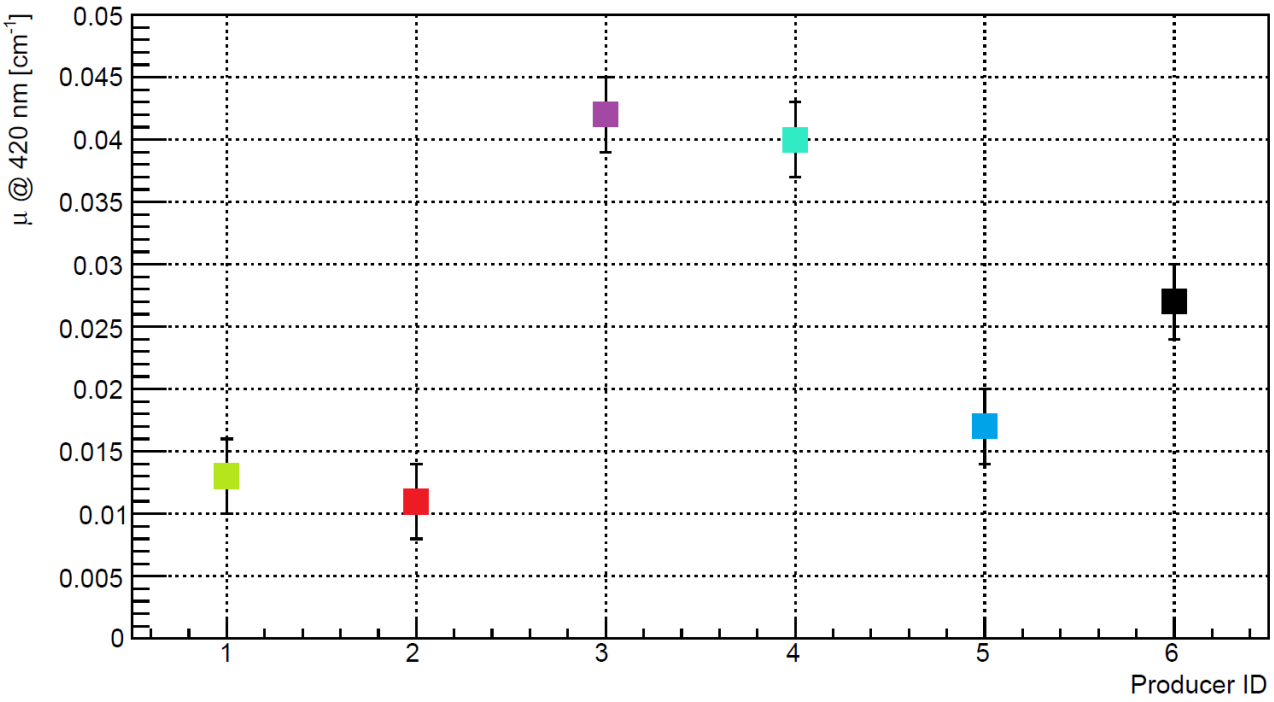

Figure 35 - Radiation induced absorption coefficient at 420 nm, for 50 kGy absorbed dose, for the irradiated samples.

By the analysis of the presented data, the crystals produced by P03 and P05 vendors seem to be more damaged by radiation. It was demonstrated that cerium is responsible for the crystal radiation hardness [6] [8], in particular (Section 2.1.3) the equilibrium between $Ce^{3+}$and Ce^{4+} ions involves the radiation-induced free electrons and holes recombination. For this reason, in the present research is of paramount importance to correlate the optical features of the sample with the cerium dopant presence in the crystal matrix.

As previously discussed, transversal transmittance measurements (below 380 nm) provide qualitative and useful information about the quantity of cerium in the analysed samples. Referring to Fig. 24, focused on the range in which Ce^{3+} absorption peak occurs (330-380 nm), the crystals that show lower quantity of dopant are precisely P03 and P05, confirming the effectiveness of the model where cerium ions act as radiation-induced free charges capture sites.

2.3.2 Photoluminescence measurements after irradiation

The PL spectra and 2D-maps of all the crystals were measured after irradiation. No differences in PL intensities and in peak positions and shapes were observed, as reported in Fig. 36 for crystal P01-BC031, as an example.

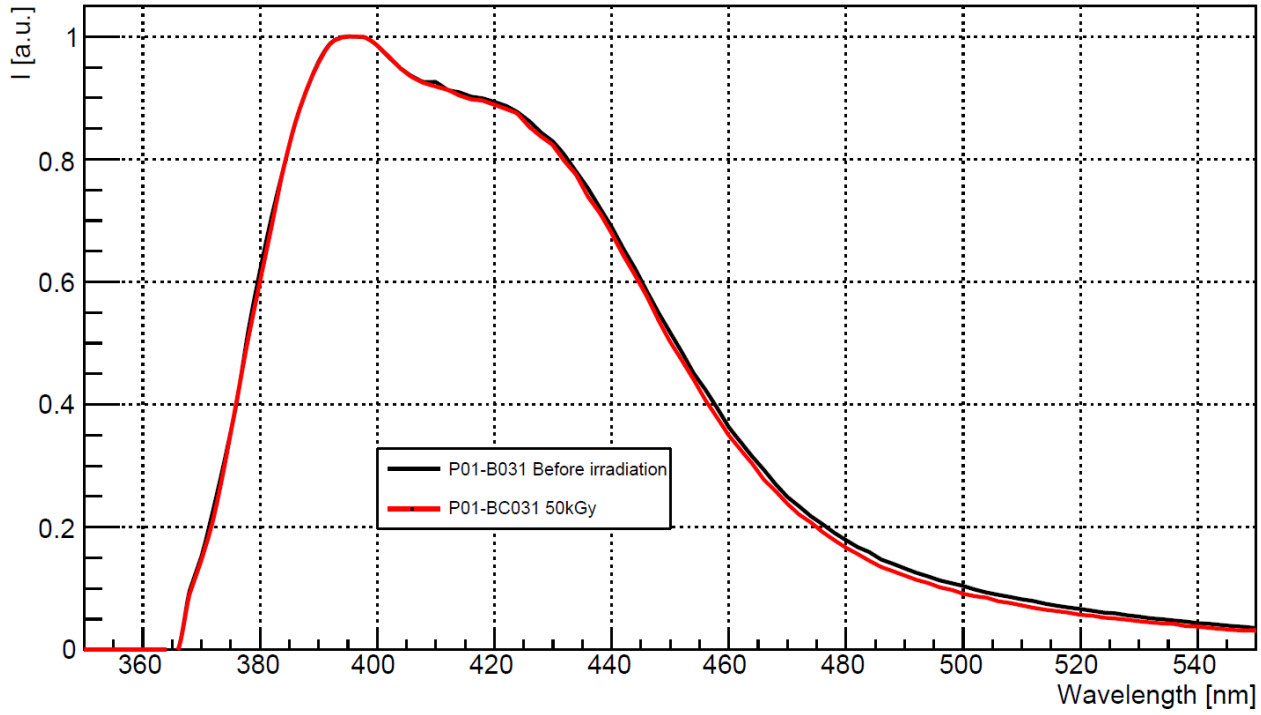

Figure 36 - Normalized emission spectra of P01-BC031 crystal before and after irradiation at 50 kGy absorbed dose.

This is a confirmation that the gamma irradiation does not affect the scintillation mechanism in these crystals.

In order to obtain the spectra in energy scale, the following conversions were applied:

$$E = \frac{hc}{\lambda} \tag{20}$$

$$I(E) = \frac{hc}{\lambda^2} I(\lambda) \tag{21}$$

where $I(E)$ and $I(\lambda)$ are the intensity in energy and wavelength scale, respectively. The PL spectra, as a function of energy [eV], can be fitted by two gaussian (Fig. 37).

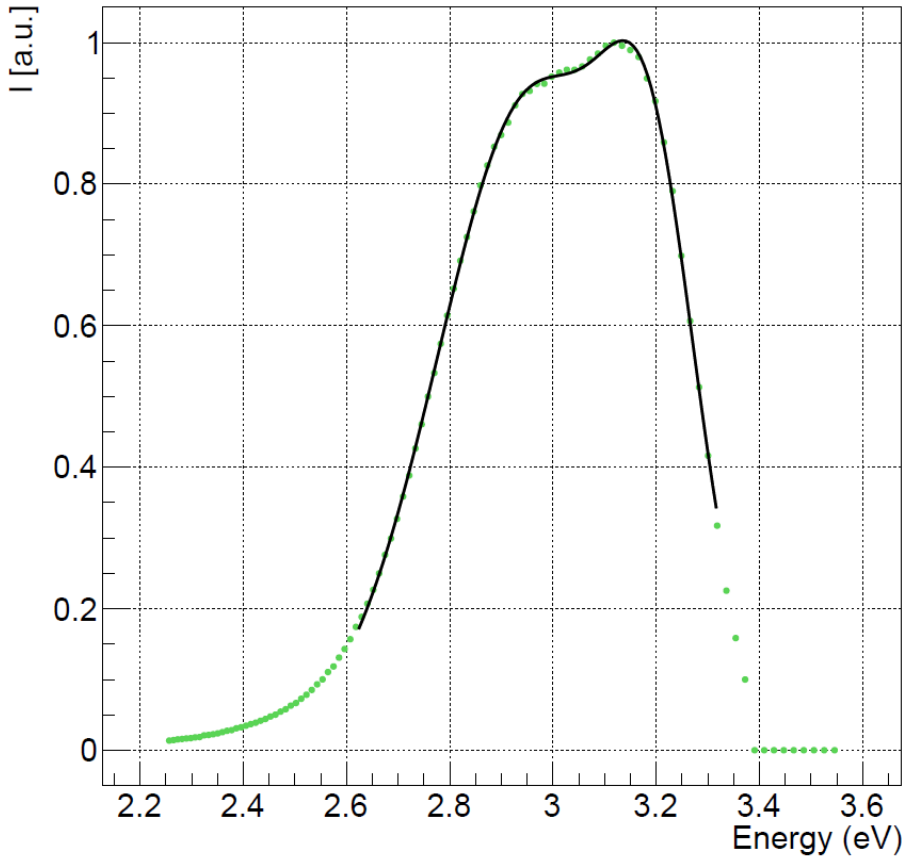

Figure 37 - Normalized emission spectra of P06 crystal fitted by a double gaussian.

The fit was performed for all the crystals. The range 2.95 - 2.97 eV cover the positions of the lower energy peak of each vendor; the peaks at higher energy are in the range 3.18 - 3.20 eV. The peaks positions are compatible within the error. The two peaks are due to the transition $5d \rightarrow 4f$ of Ce^{3+}.

2.4 Recovery tests

Studies about annealing treatments, such as dark annealing (D.A., i.e. samples kept in the dark at room temperature) and thermal annealing, are of great importance for the understanding of recovery of the defects induced by radiation [2]. Annealing treatments can restore the damaged crystals to their unirradiated state [17], by promoting the rearrangement of trapped electrons and holes.

To study the behaviour and the stability of irradiated crystals optical properties (transmittance and photoluminescence), up to two months after the end of irradiation, optical spectroscopy measurements were carried out. In particular, a first treatment was done by keeping the samples in the dark at room temperature, until no further transmittance recovery was observed (around one month of D.A.). Afterwards, the same crystal was submitted to a thermal annealing treatment at 300 °C for 16 hours to verify further transmittance recovery.

2.4.1 Annealing in the dark

The transmittance spectra recorded for P01, P02, P03, P05, P07 and P09 crystals, indicate that the recovery in the dark occurs in the first five days after the end of irradiation in term of %T and blue shift. The P07-BC133 transmittance behaviour is shown in Fig. 38 as an example. In the following month the spectra remained unchanged.

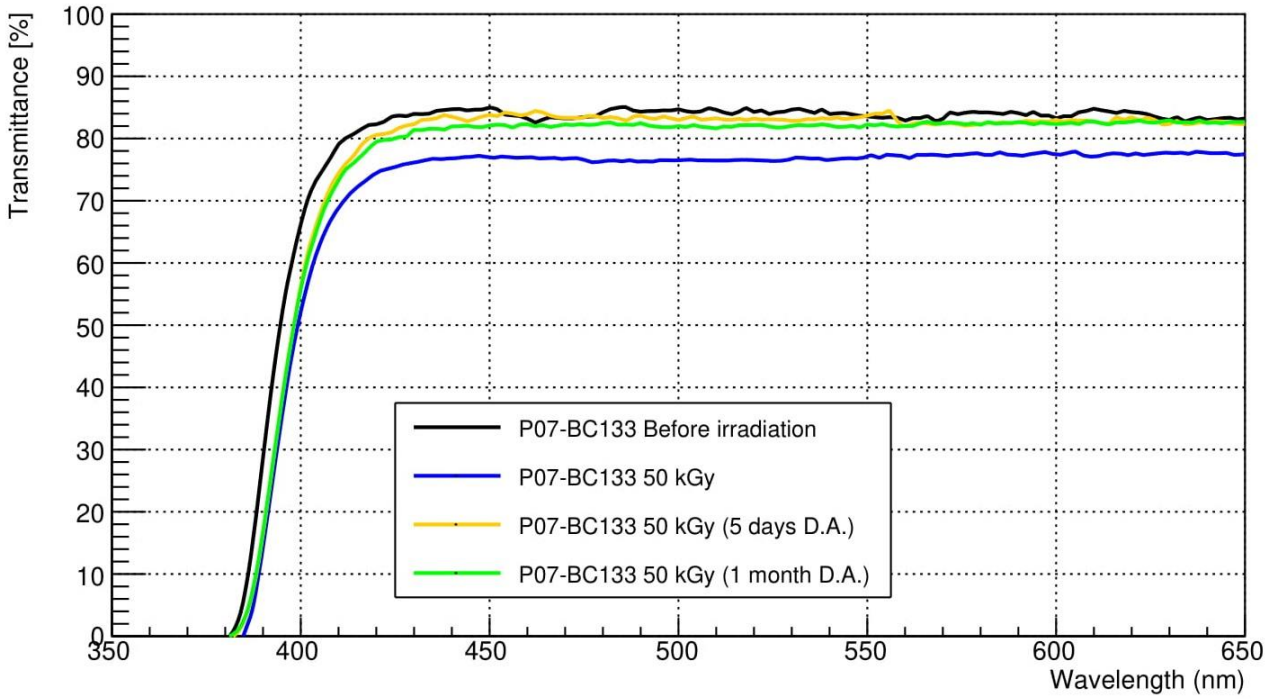

Figure 38 - Annealing in the dark of P07-BC133. Transmittance spectra before irradiation (black curve), after irradiation at 50 kGy (blue curve), after 5 days of dark recovery (yellow curve) and after 1 month of dark recovery (green curve).

2.4.2 Thermal annealing

The results obtained by transmittance measurements of crystals after the thermal treatment confirm almost a complete recovery in term of %T while this processes is ineffective for a total blue shift recovery as shown for P05-BC075 in Fig. 39 as an example.

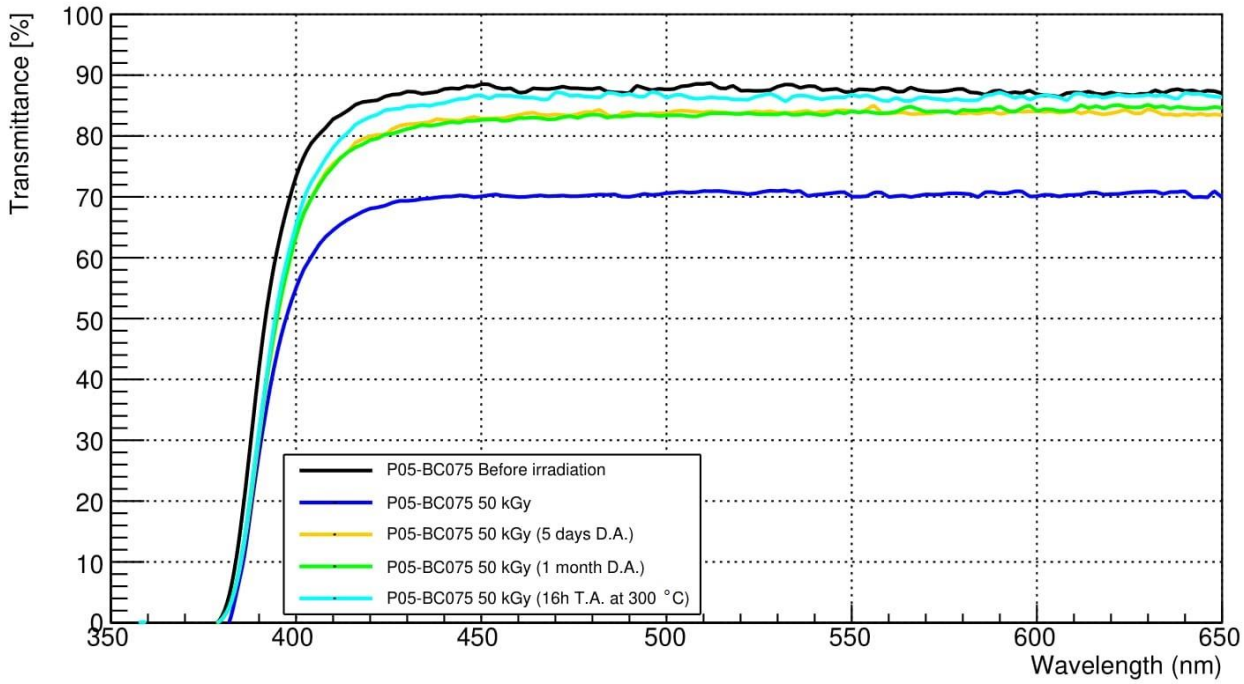

Figure 39 - Transmission spectra of P05-BC075 before irradiation (black curve), after irradiation at 50 kGy (blue curve), after 5 days of dark recovery (yellow curve) after 1 month of dark recovery (green curve) and after 16 hours of thermal annealing (T.A.) at 300 °C (light blue curve).

The values of λ_{cutoff} and of transmittance percentage for each crystal, before irradiation, after irradiation at 50 kGy, after 1 month of dark recovery and after 16 hours of thermal annealing at 300 °C, are summarized in Tab. 8.

Table 8 - Transmission spectrum parameters of crystals from vendors P01, P02, P03, P05, P07 and P09 before irradiation, after irradiation at 50 kGy, after one month of dark recovery at room temperature and after 16 hours of thermal annealing at 300°C. λ_{cutoff} error is 1 nm, %T error is 1.8.

P01-BC031	$\boldsymbol{\lambda_{cutoff}}$	**%T (420 nm)**	**T (600 nm)**
Before irradiation	387	79.2	82.2
After irradiation (50 kGy)	391	73.7	79.2
After 1 month	390	78.2	83.9
After T.A.	390	79.0	84.1
P02-BC037	$\boldsymbol{\lambda_{cutoff}}$	**%T (420 nm)**	**T (600 nm)**
Before irradiation	387	79.2	82.2
After irradiation (50 kGy)	391	73.7	79.2
After 1 month	390	79.8	83.3
After T.A.	390	81.1	83.9
P03-BC052	$\boldsymbol{\lambda_{cutoff}}$	**%T (420 nm)**	**T (600 nm)**
Before irradiation	379	82.8	84.9
After irradiation (50 kGy)	383	72.7	78.6
After 1 month	382	78.6	83.3
After T.A.	382	80.6	85.7
P05-BC074	$\boldsymbol{\lambda_{cutoff}}$	**%T (420 nm)**	**T (600 nm)**
Before irradiation	380	85.7	86.9
After irradiation (50 kGy)	383	68.1	70.1
After 1 month	382	79.3	84.1
After T.A.	382	83.1	86.5
P07-BC133	$\boldsymbol{\lambda_{cutoff}}$	**%T (420 nm)**	**T (600 nm)**
Before irradiation	383	82.3	83.3
After irradiation (50 kGy)	385	74.5	77.6
After 1 month	385	79.5	82.3
After T.A.	385	79.5	82.6
P09-BC143	$\boldsymbol{\lambda_{cutoff}}$	**%T (420 nm)**	**T (600 nm)**
Before irradiation	386	81.6	86.4
After irradiation (50 kGy)	390	69.9	76.5
After 1 month	389	74.3	83.2
After T.A.	389	75.7	83.4

Thermal treatment is also suggested in literature [7] for not irradiated crystals. For this reason, two samples (P05-BC074 and P05-BC076) of the same vendor, with equal transmittance before irradiation, were chosen to verify the effect of the thermal annealing on the crystal behaviour under irradiation. In particular, a thermal annealing at 300 °C for 16 hours was applied to the P05-BC076 crystal before irradiation at 43 kGy. The transmittance curves of the sample were reported in Fig. 40. In the same figure, the spectra of the sample P05-BC074 before and after irradiation at 43 kGy absorbed dose were shown. These preliminary results indicate that the thermal treatment, performed before irradiation, improves the radiation hardness of the crystals. In order to confirm it, further studies will be performed on other samples.

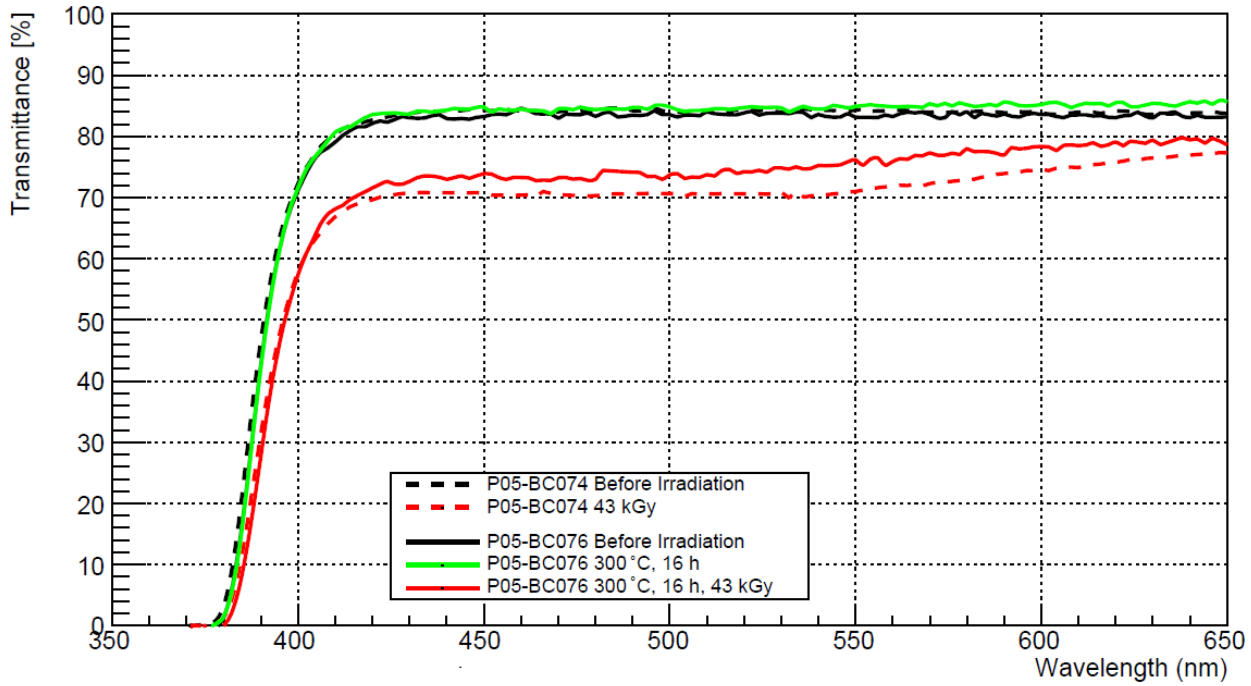

Figure 40 - P05-BC074 (dashed curves) and P05-BC076 (solid lines) transmission spectra. Before irradiation curves are the black ones, after irradiation are the red ones and the green curve is the one after thermal annealing at 300 °C for 16 hours.

The parameters referred to the P05-BC074 and P05-BC076 crystals transmission spectra are summarized in Tab. 8.

Table 9 - Transmission spectrum parameters of two crystals from vendor P05 on which the annealing treatment was performed after irradiation (P05-BC075) and before irradiation (P05-BC076). λ_{cutoff} error is 1 nm, %T error is 1.8.

P05-BC074	λ_{cutoff}	**%T (420 nm)**	**T (600 nm)**
Before irradiation	380	83.0	84.6
After irradiation (43 kGy)	382	69.6	74.6
P05-BC076	λ_{cutoff}	**%T (420 nm)**	**T (600 nm)**
Before irradiation	380	81.9	83.2
After 16 h T.A. at 300 °C	380	83.6	85.2
After irradiation (43 kGy)	382	71.6	78.3

In conclusion, the analysed LYSO:Ce crystals show good radiation resistance after irradiation at 50 kGy absorbed dose. Indeed, their PL spectra do not change in intensity, peak position and shape, after irradiation. Their transmission spectra after irradiation, show a slight redshift and a decrease which is almost completely recovered after 5 days of dark annealing.

From preliminary study carried out in this work and elsewhere reported in literature [7], thermal annealing treatment performed before irradiation seems to be effective in improving the crystals radiation hardness.

Conclusion

LYSO:Ce crystals are widely employed in radiation detection and they are characterized by small rise and decay time, high light yield, good radiation resistance and high density, i.e. short radiation length. Furthermore, this kind of scintillators is widely used for PET applications, thus a large number of producers are available, but not qualified for high radiation environment such as High Energy Physics (HEP) experiments.
In this work, LYSO:Ce crystals from different producers were analysed. In particular, irradiation tests and optical spectroscopic characterization at the Calliope gamma irradiation facility (ENEA, Casaccia R.C.) were performed.

In order to test the radiation resistance of LYSO:Ce crystals from six different vendors, irradiation tests up to 50 kGy absorbed dose were performed. The results obtained by longitudinal and transversal transmittance measurements show a slight red shift and a decrease of transmittance after gamma irradiation for all crystals in the whole analysed range (350-650 nm). The effect of cerium ions added as dopant to improve the radiation hardness of the crystal matrix was also analysed. The obtained results indicate an higher radiation damage for a couple of vendors crystals characterized by lower amount of dopant, confirming the effectiveness of cerium ions as radiation-induced free charges capture sites.
Studies about annealing treatments, such as dark and thermal annealing (16 hours at 300 °C), were carried out to investigate the possibility of recovering the damaged crystals. The recovery in the dark occurs in the first five days after the end irradiation: the crystals partially recover in transmittance percentage but not in blue shift.
The thermal treatment gives the complete recovery in term of %T while this process has no effect on the blue shift. The analysed LYSO:Ce crystals show good radiation resistance after irradiation at 50 kGy absorbed dose. Thus, LYSO:Ce crystals are suitable also for high radiation environment.
In order to evaluate the effect of irradiation on LY and DT measurements, further studies will be carried out. LY and DT have already been measured after irradiation at a dose rate of 1 Gy/h, for few hours, and no effect on LY and DT was observed.
Photoluminescence (PL) measurements, in which the excitation is due to the absorption of photons from a source of light, are a very useful tool for the study of luminescence centres involved in the scintillation process. PL data show negligible differences in intensity, peak position and band shape after irradiation.

References

[1] S. Gundacker, R.M. Turtos, E. Auffray, and P. Lecoq. Precise rise and decay time measurements of inorganic scintillators by means of x-ray and 511 kev excitation. *Nuclear Instruments and Methods in Physics Research Section A: Accelerators, Spectrometers, Detectors and Associated Equipment* **891** (2018) P42.

[2] S. Baccaro. *Scintillating crystal Working principles of scintillation and techniques of characterization*. ENEA, Roma, 2006.

[3] S. Blahuta, A. Bessiere, and B. Viana. Defects Identification and Effects f Annealing on $Lu_{1-x}Y_{2x}SiO_5$ (LYSO) Single Crystals for Scintillation Application *Materials (Basel)* **4(7)** (2011) P1224

[4] M. Nikl and A. Yoshikawa. Recent R&D trends in inorganic single-crystal scintillator materials for radiation detection. *Advanced Optical Materials* **3(4)** (2015) P463.

[5] P.A. Rodnyi. *Physical Processes in Inorganic Scintillators*. Laser and Optical Science and Technology Series. CRC Press, Boca Raton, FL, 1997.

[6] S. Baccaro, A. Cecilia, A. Cemmi, E. Mihokova, M. Nikl, K. Nitsch, P. Polato, G. Zanella, and R. Zannoni. Colour centres induced by γ irradiation in scintillating glassy matrices for middle and low energy physics experiments. *Nuclear Instruments and Methods in Physics Research Section B: Beam Interactions with Materials and Atoms* **185(1)** (2001) P294.

[7] S. Baccaro, A. Cecilia, and E. Mihokova. Radiation damage induced by γ irradiation on Ce^{3+} doped phosphate and silicate scintillating glasses. *Nuclear Instruments & Methods in Physics Research, Section A Accelerators Spectrometers Detectors and Associated Equipment* **476(3)** (2002) P785.

[8] S. Baccaro, A. Cemmi, I. Di Sarcina, and F. Menchini. Gamma rays effects on the optical properties of cerium-doped glasses. *International Journal of Applied Glass Science* **6** (2015) P295.

[9] B. McGrath, H. Schoenbacher, and M. Van de Voorde. Effects of nuclear radiation on the optical propertiesof cerium-doped glass. *Nuclear Instruments and Methods* **135(1)** (1976) P93.

[10] M. Brandily-Anne, J. Lumeau, L. Glebova, and L. Glebov. Specific absorption spectra of cerium in multicomponent silicate glasses. *Journal of Non-crystalline Solids* **356** (2010) P2337.

[11] M. Moszynki, M. Kapusta, M. Mayhugh, D. Wolski and S.O. Flyckt. Absolute Light Output of Scintillators. *IEEE Transactions on nuclear science* **44(3)** (1997) P1052.

[12] S. Baccaro, A. Cemmi, I. Di Sarcina, and G. Ferrara. *Gamma Irradiation Calliope Facility at ENEA - Casaccia research centre (Rome, Italy)*. ENEA, Roma, 2019.

[13]] M. Nikl and A. Yoshikawa. Review of luminescent properties of Ce^{3+} doped garnet phosphors: New insight into the effect of crystal and electronic structure. *Optical Materials: X* **1** (2019) P100018.

[14] R. Mao, L. Zhang, and R. Zhu. Optical and scintillation properties of inorganic scintillators in high energy physics. *IEEE Transactions on Nuclear Science* **55(4)** (2008) P2425.

[15] D. Ma and R. Zhu. Light attenuation length of barium fluoride crystals. *Nuclear Instruments* & *Methods in Physics Research Section A-accelerators Spectrometers Detectors and Associated Equipment* **333** (1993) P422.

[16] J. Chen, L. Zhang, and R. Zhu. Large size lyso crystals for future High Energy Physics experiments. *IEEE Transactions on Nuclear Science* **52(6)** (2005) P3133.

[17] A. Rossi. *Caratterizzazione di Cristalli di LYSO per Esperimenti di Fisica delle Alte Energie*. Tesi di Laurea, 2007-2008.

[18] M. Chowdhury and D. Imrie. Thermal annealing and optical darkening effects in CsI(Tl) crystals. *Nuclear Instruments and Methods in Physics Research Section A: Accelerators, Spectrometers, Detectors and Associated Equipment* **432(1)** P138.

ENEA
Servizio Promozione e Comunicazione
www.enea.it

Stampa: Laboratorio Tecnografico ENEA - C.R. Frascati
gennaio 2021